Economic Nonlinear Predictive Control for Real-Time Optimal Energy Management of Parallel Hybrid Electric Vehicles

JINSUNG KIM[1], HOONHEE KIM[1], JINWOO BAE[1], DOHEE KIM[2], JEONG SOO EO[2], (Member, IEEE), AND KWANG-KI K. KIM[1]

[1]Department of Electrical and Computer Engineering, Inha University, Incheon 22212, South Korea
[2]Electrified Systems Control Research Laboratory, Research and Development Division, Hyundai Motor Company, Hwaseong 18280, South Korea

Corresponding author: Kwang-Ki K. Kim (kwangki.kim@inha.ac.kr)

ABSTRACT This article presents an economic nonlinear hybrid model predictive control strategy for optimal energy management of parallel hybrid electric vehicles. Hybrid electric vehicles are controlled for operation in various driveline modes and the associated optimal control problem involves both continuous and discrete control variables. To solve the resultant mixed-integer nonlinear optimal control problem, we propose a hierarchical supervisory control architecture that consists of demand prediction, driveline mode determination, and real-time optimization. These three modules are designed independently and connected in series to perform computer-aided control. The demand prediction module uses a times series model to forecast the mechanical traction power requests of the driver over a prediction horizon based on vehicle speed, road grade, acceleration pedal scale, brake pedal scale, and past and current power demands. For a given forecasted power demand profile, the mode determination module decides a sequence of driveline modes that are presumed to be operated over the prediction horizon. The model-based real-time optimization corresponding to nonlinear model predictive control computes the optimal motor power over a prediction horizon, and the receding horizon scheme as feedback control is applied to repeat the processes of the three control modules. A dedicated case study with real driving data obtained from Hyundai IONIQ PHEV 2018 is presented to demonstrate the effectiveness in fuel economy and emission reduction offered by the proposed optimal energy management strategy. The proposed hierarchical real-time predictive optimization-based strategy is competitive with any exiting power management strategies such as dynamic programming and equivalent consumption minimization strategy in fuel economy and emission reduction while showing better charge-sustaining capability. This trade-off between fuel economy and charge-sustainability can be further improved by tuning the hyper-parameters in the proposed optimal control problem.

INDEX TERMS Optimal energy management, parallel hybrid electric vehicle, model predictive control (MPC), mode transition control, Pontryagin's minimum principle (PMP), equivalent consumption minimization strategy (ECMS).

NOMENCLATURE

V_{oc}	Open-circuit voltage of a battery
R_{T}	Internal resistance of a battery
ξ	State of charge (SOC) of a battery
P_m	Motor power (mechanical)
P_b, P_l	Batter power and power loss in a battery (electrical)
P_e, P_f	Engine power (mechanical) and fuel power (chemical)
$\hat{P}_d$	Predicted demand power (mechanical)
I_b, V_b	Current and voltage of a battery
α	Battery power loss coefficient
e, η	Engine and motor efficiency
$V_{b,\min}, V_{b,\max}$	Minimum and maximum of V_b
$\xi_{\min}, \xi_{\max}$	Minimum and maximum of ξ
ξ_0	Initial value of SOC

The associate editor coordinating the review of this manuscript and approving it for publication was Ton Duc Do.

$P_{m,\min}, P_{m,\max}$	Minimum and maximum motor power
$P_{e,\max}$	Maximum engine power
t_0, t_f, t_s	Initial, terminal, and sampling time
δ	Driveline mode
χ	State of engine clutch
N	Prediction horizon of MPC
$\dot{m}_f$	Fuel mass flow
$\dot{m}_{\mathrm{NO}_x}, \dot{m}_{\mathrm{HC}}$	Mass flow of NO_x and HC
s	Co-state variable of ECMS
K_p, K_i	Proportional and integral gain for s
P_0^{on}	Kinetic friction loss of engine
P_0^{off}	Static friction loss of engine
$q_\delta, q_{\mathrm{DP}}$	Battery charge sustaining parameter of NMPC and DP
$q_{\mathrm{NO}_x}, q_{\mathrm{HC}}$	Exhaust emission weighting parameter of NO_x and HC
BSFC	Braking specific fuel consumption of engine
w_e, w_m	Engine speed and motor speed
T_e, T_m	Engine torque and motor torque
v_d, a_d	Desired speed and required acceleration
$\gamma_{\mathrm{gear}}, \gamma_{\mathrm{final}}$	Transmission gear and final drive ratio
Q_{lhv}	Lower heating value of gasoline

I. INTRODUCTION

In recent years, as environmental pollution draws attention of people across the world and related policies are strengthened, regulations on exhaust gases of automobiles are being reinforced. Moreover, there is a growing interest in environmentally friendly energy sources (such as hydrogen and electricity) to replace fossil fuels. Consequently, research investment and interest in developing new types of vehicles with powertrain energy management strategies that consume less fossil fuel and emit fewer pollutants than conventional gasoline or diesel vehicles have been increasing steadily. These new vehicles are primarily classified into three types: battery electric vehicle (BEV), hybrid electric vehicle (HEV), and fuel-cell electric vehicle (FCEV) [1]. In particular, HEV uses an electric motor (EM) as an additional traction power source, together with an engine that is a conventional power source [2]. Consequently, the new degree of freedom achieved by distributing the required traction power demand to the engine and motor affords the HEV lower pollutant emissions than conventional vehicles while improving the fuel economy [3]. Depending on the power splitting between engine and motor, HEV has various modes of operation determined by continuous and discrete control variables [4], which result in challenges in real-time implementation of optimization-based supervisory control strategies.

The fuel economy of the HEV highly depends on the energy-management strategy that optimizes the operation between two power sources [5], [6]. The energy-management strategy of the HEV is primarily classified into three categories: rule-based, optimization-based, and learning-based [7]. The rule-based energy management strategy is typically divided into deterministic rule-based and fuzzy rule-based strategies. In general, deterministic rule-based energy management strategy is based on rules designed with regards to a discovery, intuition, or human expertise without a priori information of the driving cycle [8]. Therefore, this strategy works effectively only at certain powertrains and cannot cope with small changes in the driving conditions. Fuzzy rule-based EMS uses the concept of fuzzy logic to increase the robustness against system uncertainty [9], [10]. To improve the transient response of the engine, fuzzy gain scheduling was used in [11] to determine the appropriate parameters of the proportional–integral (PI) controller. However, these rule-based energy management strategies have a limitation in that the overall efficiency of the HEV system is low and the solution is suboptimal due to the intrinsic nature of non-inclusion of any optimization process.

The optimization-based energy-management strategy can be classified into offline optimization and online (or real-time) optimization energy-management strategies [12], [13]. The former obtains a global optimum that minimizes the cost function (such as total fuel consumption or pollutant emissions) during the entire driving cycle. This method requires a priori information of the driving cycle, and dynamic programming (DP) is representative of this method. DP is a direct discrete-time method, and it decomposes the existing optimization problem into a sequence of subproblems [12]. In this process, the value function, called optimal cost-to-go, is calculated offline via backward induction; the curse of dimensionality is among its disadvantages, wherein the amount of calculation increases rapidly based on the dimensions of the system variables [14], [15]. The advantage of DP is that the optimal policy can be determined even with nonlinear constraints, and a full range of optimal solutions can be obtained [3]. Therefore, the result of DP is typically used as a benchmark for comparing the obtained results with other methods [16]. An improved rule-based control strategy, which extracts implementable near-optimal rules by interpreting the results obtained from the DP, is presented in [17]. The determination of different hybridization ratios of two types of parallel HEV, namely, torque assist parallel HEV, and full parallel HEV using the DP algorithm is presented in [18].

Unlike the global optimization energy-management strategy, the real-time optimization energy-management strategy, such as equivalent consumption minimization strategy (ECMS) and model predictive control (MPC), can be applied to a real-time control system. The advantages of this strategy are its simple implementation and sufficient robustness to respond to sudden changes in driving conditions [5], [7]. ECMS is an approximate realization of the Pontryagin's minimum principle, and it transforms the original global optimization problem into a local optimization problem that minimizes the equivalent fuel consumption at every instant [19], [20]. The equivalent fuel consumption corresponds to the sum of the actual fuel consumption of the internal combustion engine (ICE) and fuel consumption converted from the energy storage system. The main

difficulty when implementing the ECMS is the selection of the *equivalent factor* that is associated with the driving cycle and battery state of charge (SOC). If the value of the equivalence factor is appropriately selected, the control performance improves. Therefore, research on the effective identification of the equivalence factor by predicting future driving information has been actively pursued [16]. The application of an on-line adaptation law for equivalence factor reduces the computational burden and guarantees optimality, as described in [21]. An effective penalty method using implicit Hamiltonian minimization is proposed in [22] to deal with problems involving state and input constraints. In [23], the driving cycle of a plug-in hybrid electric bus was divided into several segments based on each bus stop. The equivalence factor of each segment was optimized using linear weight particle swarm optimization algorithm. In addition, the equivalence factor oscillation problem in basic adaptive ECMS is solved by using the bisection method, which is presented in [24]. In this article, the application of ECMS to determine the operation mode of HEV is described in Section III-B.

MPC is an approach based on the receding horizon control scheme and model-based batch predictions of the behaviors of controlled dynamical systems. The MPC can be used to systematically and explicitly handle multivariate and nonlinear constrained control problems in real time [25]. In the case of the HEV, the physical equations for the control system are highly nonlinear, and the constraints on the operation of each component are also considered. Therefore, MPC is considered a suitable control method. The operation principle of the MPC can be described as follows: the optimal control sequence, which satisfies the constraint and minimizes the cost function, is calculated over the prediction horizon; the first term of the calculated optimal control sequence is considered; and this procedure is repeated at the next step [26]. The nonlinear and constrained optimal control problem of power-split HEV is solved by using nonlinear MPC with short prediction length, which improves fuel economy and enables online calculation [27]. The results of using MPC for energy management of hybrid electric tracked vehicles are compared with the results of the rule-based strategy and DP in general driving conditions [28]. The integrated power management of plug-in HEV (PHEV) with multiple energy sources is shown in [29]. In particular, MPC was used to determine the output power between the battery pack and ultracapacitor pack of the hybrid energy storage system, and DP was also applied to optimize the battery output current. Based on three test driving cycles, the robustness of the proposed method was verified. In this article, the formulation of the economic nonlinear MPC for optimal energy-management of the parallel HEV is described in Section III-C.

Lastly, a learning-based energy management strategy, such as reinforcement learning, enables the self-adaptation for different driving environments through learning from historical driving data [7]. Therefore, research on the power distribution of HEV is underway using this strategy because of the advantage that future driving information is unnecessary [30]–[32].

Reinforcement learning is a type of machine learning in which an agent learns based on rewards gained through interactions with its environment. In general, it is a set of algorithms (e.g., temporal difference(TD)-learning, Q-learning, and deep Q Network) to solve problems represented as Markov decision processes [15], [33]. Lin *et al.* [30] applied a TD(λ)-learning algorithm with a high convergence rate and performance even in a non-Markovian environment to power management of parallel HEV. The application of deep Q-learning to a power-split hybrid electric bus using a deep neural network to approximate Q functions is described in [34]. Upon comparing the proposed deep Q-learning-based strategy with Q-learning, the performance was found to be improved in terms of computation time and convergence rate in case of the former. Han *et al.* [35] proposed double deep Q-learning to prevent policy estimates from falling into overoptimistic. The efficiency of the proposed method is verified by comparison with conventional deep Q-learning and DP.

In addition to the fuel efficiency, the important factors to consider in energy energy management strategy for HEV are reduction of exhaust emission and extension of battery life. As the real driving NO_x emission of a typical diesel-engine vehicle does not comply with the regulations for exhaust emission, the authors of [36] presents an ECMS method considering real driving NO_x emission of diesel-engine HEV. In a hardware-in-the-loop experiment, they show that compared to a conservative non-adaptive strategy to meet the emission regulation, their ECMS-based method results in a 7% improvement in fuel consumption. Another approach to minimize the drivetrain cost, fuel consumption, and exhaust emissions simultaneously is proposed in [37] that uses a multi-objective particle swarm optimization technique. In [38], a genetic fuzzy control scheme is proposed to exploit traffic condition recognition and prediction for the purpose of minimizing both fuel consumption and exhaust emission.

To avoid the frequent charging and discharging of electric vehicles and to maximize regenerative braking energy, the authors of [39] proposed a new hybrid energy storage system. The multi-objective optimization problem for PHEV considering energy consumption and battery health at the same time is solved by using stochastic dynamic programming and particle swarm optimization [40]. At this time, a semi-empirical model considering the effects of battery temperature and SOC was used as the battery lifetime model. To describe the propagation of aging and life-span of advanced energy storage systems, a control-oriented battery pack model is proposed in [41]. The model predicts battery pack aging, thermal, and electrical dynamics under actual PHEV operation.

The main contributions of this study are summarized below.

- To overcome some limitations and drawbacks in existing energy management strategies for parallel hybrid electric vehicles, we present a modularized hierarchical supervisor control architecture.

- Three modules are designed independently and connected in series to perform computer-aided control, so the proposed method is scalable.
- The model-based real-time optimization corresponding to the economic NMPC satisfies the sophisticated operating limits of the high-voltage battery, and the receding horizon scheme as feedback control is applied to repeat the processes.
- A regression model for exhaust emission was included in the objective function to minimize fuel consumption and to comply with environmental pollutant legislation.
- In this hierarchical architecture of supervisory control, one can reduce the burden of real-time computation by separating online and offline analysis and design and increase reliability by redundancy and backup role of the ECMS and MPC modules.
- As opposed to the most existing ECMS methods, the rule for determining the powertrain operation mode explicitly considers the engine efficiency obtained from a commercial PHEV engine so that the optimality of fuel-economy could be further improved.

The remainder of this article is organized as follows: Section II describes the typical parallel HEV architecture and the proposed simplified model. In Section II, mathematical modeling of the operating constraints of the battery and powertrain and the optimal control problem formulation for optimizing fuel economy are presented. In Section III, a novel hierarchical supervisory control that consists of the power demand predictor, mode determiner, and real-time optimization modules is detailed. An explanation of different operation modes based on the ECMS is provided in Section III-B. Section III-C presents the solution of the optimal control problem presented in Section II using the nonlinear MPC based on the operation mode determined by the ECMS. In Section IV, the effectiveness of the proposed method is demonstrated by comparing the results with the ones of DP solution and ECMS. For a case study, we use actual commuting driving data obtained from a commercial PHEV. Finally, the conclusions and future work are provided in Section V.

II. OPTIMAL CONTROL PROBLEM FOR ENERGY MANAGEMENT OF PARALLEL HEV

In this section, we formulate the hybrid optimal control problem in which control variables have both continuous and discrete values for optimal energy management of the parallel HEV [4]. To formulate the problem, we first present power-flow equations that describe the power links in the driveline of a parallel HEV and the battery-state changes. In addition, we consider the operating limits of the battery that impose the state and control input constraints in the optimal control problem corresponding to optimal energy management and physical limits of engine and motor. The resultant optimal control problem is formulated as an economic nonlinear MPC in Section III-C wherein the control input is the only continuous variable. Furthermore, the cost function is divided
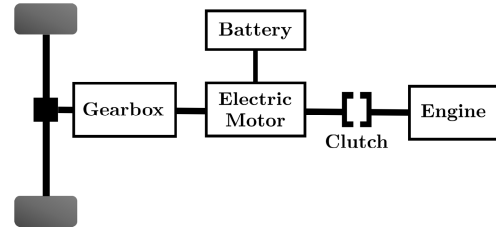

FIGURE 1. Driveline architecture of parallel HEV.

into two parts, namely, fuel usage, and battery usage, and constraints are introduced corresponding to the operating limits of the battery, engine, and motor.

A. DYNAMICAL SYSTEM EQUATIONS

In the parallel HEV, the ICE and EM are connected in parallel to deliver the generated power to the wheel. As shown in Figure 1, the clutch between the engine and motor controls the engine power as required. Therefore, when the power demand is low, the motor operates alone, and when it is high, the ICE operates alone. If the required power is higher than the maximum power produced by the engine, the ICE operates at the optimal operating line and uses the motor to generate additional power. In the case of regenerative braking, the EM acts as a generator to charge the battery.

1) LONGITUDINAL VEHICLE DYNAMICS

The longitudinal dynamics of the vehicle is represented by [3], [42]:

$$
\begin{aligned}
F_{\text{trac}} &= M_{eqv}\frac{dv_d}{dt} + F_{\text{aero}} + F_{\text{grade}} + F_{\text{rolling}} \\
&= M_{\text{eqv}}a_d + \frac{1}{2}\rho A_f c_d v_d{}^2 + M_v g \sin(\theta_{\text{grade}}) \\
&\quad + c_r M_v g \cos(\theta_{\text{grade}})
\end{aligned} \tag{1}
$$

where F_{trac} is traction force, F_{aero} is aerodynamic drag force, F_{grade} is gravitational force, and F_{rolling} is rolling resistance force. ρ is air density, A_f is the aerodynamic frontal area, c_d is drag coefficient, c_r is rolling friction coefficient, g is gravitational acceleration, θ_{grade} is the road slope. The equivalent mass M_{eqv} is represented as

$$
M_{\text{eqv}} = M_v + \frac{(J_w + \gamma^2 J_m)}{r_w{}^2}
$$

where M_v is vehicle mass, J_w, J_m is the inertia of wheel and motor, respectively. γ is constant gear ratio, r_w is wheel radius. In general, the equivalent mass slightly varies with the gear ratio γ_{gear}, but in this article, a constant gear ratio is used for convenience. Table 1 shows a list of vehicle parameters that are used for case studies presented in this article.

For a given driver's desired speed profile, the required acceleration is approximated as

$$
a_d(t) \approx \frac{v_d(t + \Delta t) - v_d(t)}{\Delta t} \tag{2}
$$

TABLE 1. Vehicle parameter corresponding to the longitudinal dynamics.

Parameter	Value	Unit
M_v	1800	kg
J_w	4.78	kg·m^2
J_m	0.0435	kg·m^2
A_f	2.408	m^2
c_d	0.24	-
c_r	0.01	-
ρ	1.2754	kg/m^3
g	9.81	m/s^2
r_w	0.32	m
γ	4.5	-
γ_{gear} (1st to 4th)	[3.867, 2.217, 1.371, 0.930]	-
γ_{gear} (5th to 6th)	[0.956, 0.767]	-
γ_{final} (1st to 4th)	4.188	-
γ_{final} (5th to 6th)	3.045	-

that is assumed to be constant over the interval $[t, t + \Delta t]$. If a desired speed profile is given over a time interval $[0, T]$, then the required acceleration profile can be calculated through (2) and the traction force can be obtained based on the longitudinal dynamics (1). The mechanical power demand for longitudinal traction is computed by

$$P_d(t) = F_{\text{trac}}(t) \, v_d(t) \quad \text{for } t \in [0, T]. \tag{3}$$

For the implementation and experiment of supervisory control strategies of HEV with driving cycles, the power demand for longitudinal traction is calculated by the above procedure. This process of power demand calculation will be further explained in Section IV-D1.

2) BATTERY MODEL

The battery is a reversible electrochemical energy storage device and is a key element of an HEV. In the powertrain, we consider a traction battery that is characterized in terms of its power and capacity. The battery power and battery current, denoted by P_b and I_b, must match the power links of the electrical path for a given power demand requested by the driver. The battery capacity, denoted by Q, must satisfy the desired driving-operation specifications. The nominal battery capacity, denoted by Q_{nom}, is the integral of battery current that can be delivered by a fully charged battery when completely discharged under a certain nominal condition.

Battery modeling in HEV energy management is primarily aimed at predicting the changes in SOC or electrical energy when the driving power demand, battery power, and motor power are given. To describe and monitor the battery state, we consider a dimensionless parameter, denoted by ξ, that is defined as the ratio of current capacity to nominal capacity:

$$\xi(t) = \frac{Q(t)}{Q_{\text{nom}}} \tag{4}$$

Direct measurement of $Q(t)$ is not possible in automotive-battery-management systems. Instead, the time rate of the battery charge is approximated by the balance equation [43], [44]

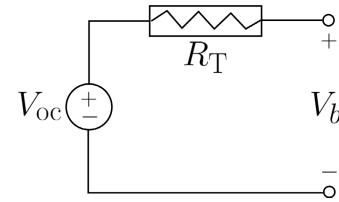$$\frac{dQ}{dt}(t) = -\frac{I_b(t)}{\eta_c^{\text{sign}(I_b(t))}} \tag{5}$$

FIGURE 2. Equivalent circuit of a battery in steady-state.

where I_b is positive when the battery discharges, and it is negative when it charges. The parameter η_c denotes a charging or Coulombic efficiency, which models a fraction of the current I_b that can be actually transformed into charge in the battery. The function $\text{sign}(I_b)$ has the values 1, -1, and 0 for $I_b > 0$, $I_b < 0$, and $I_b = 0$, respectively.

A simplified model of a battery can be the equivalent circuit shown in Figure 2 that corresponds to the circuit in steady-state. The open-circuit voltage and internal resistance in the equivalent circuit are described by $V_{\text{oc}}(\xi(t))$ and $R_{\text{T}}(\xi(t))$ that primarily depend on the SOC. The regression of dependency was performed in the form of a polynomial function of the measured data. As the degree of the polynomial function increases, there is a trade-off relationship in which the complexity of the model increases but the root mean square error (RMSE) decreases. In this study, the order of regression is set to five, considering that the RMSE for $V_{\text{oc}}(\xi(t))$ and $R_{\text{T}}(\xi(t))$ are improved by 26.8% and 36.1%, respectively, when it changes from four to five. The dependencies are shown in Figure 3.

Using Kirchhoff's voltage law with a passive sign convention, we obtain the following equations:

$$P_b(t) = V_{\text{oc}}(\xi(t))I_b(t) - R_{\text{T}}(\xi(t))I_b^2(t) \tag{6}$$

and

$$I_b(t) = \frac{V_{\text{oc}}(\xi(t))}{2R_{\text{T}}(\xi(t))} - \sqrt{\frac{V_{\text{oc}}^2(\xi(t))}{4R_{\text{T}}^2(\xi(t))} - \frac{P_b(t)}{R_{\text{T}}(\xi(t))}} \tag{7}$$

Combining the equations (4), (5), and (7), we obtain a nonlinear differential equation for the battery SOC

$$\frac{d\xi}{dt}(t) = F(\xi(t), P_b(t)) \tag{8}$$

$$= \frac{1}{\eta_c^{\text{sign}(P_b(t))} Q_{\text{nom}}}$$

$$\times \left(\frac{\sqrt{V_{\text{oc}}^2(\xi(t)) - 4R_{\text{T}}(\xi(t))P_b(t)} - V_{\text{oc}}(\xi(t))}{2R_{\text{T}}(\xi(t))} \right) \tag{9}$$

and the power dissipated in the battery is given by

$$P_\ell(t) = R_{\text{T}}(\xi(t))I_b^2(t)$$

$$= \frac{\left(\sqrt{V_{\text{oc}}^2(\xi(t)) - 4R_{\text{T}}(\xi(t))P_b(t)} - V_{\text{oc}}(\xi(t)) \right)^2}{4R_{\text{T}}(\xi(t))} \tag{10}$$
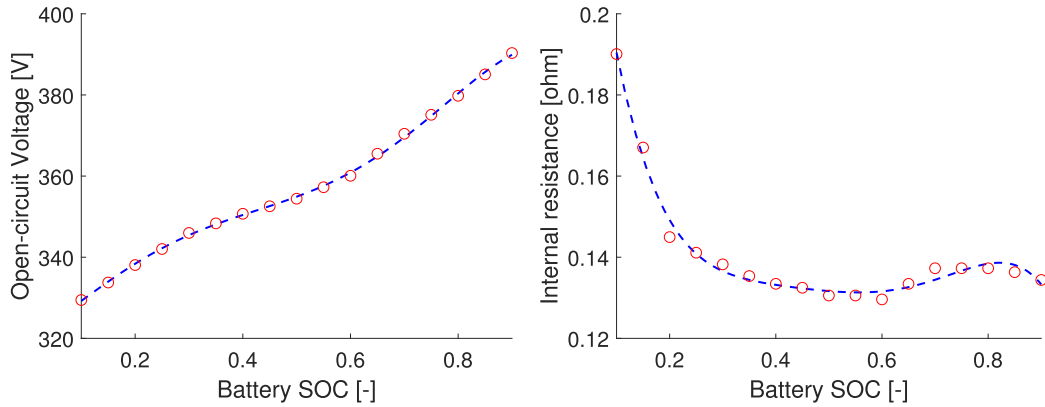
FIGURE 3. Polynomial regression is used for the open-circuit voltage (V_{oc}) and internal resistance (R_T) for an equivalent circuit model of a real-world high-voltage battery used in a commercial PHEV. The red dots and dashed lines indicate measured data and polynomial regression, respectively.
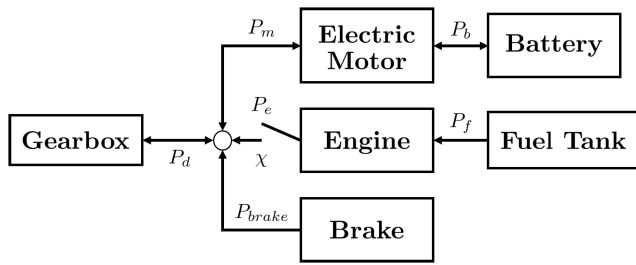

FIGURE 4. The topology of power flow and links in parallel HEV.

3) ELECTRIC POWER LINKS

The topology of power flow and links in the driveline of a parallel HEV are shown in Figure 4. The variable $\chi \in \{0, 1\}$ refers to the state of the engine clutch; $\chi = 1$ implies that the engine is clutched, whereas $\chi = 0$ implies the engine is disengaged from the driveline. The brake operates in certain situations, such as when the power demand is lower than the minimum of motor power or to prevent overcharging. At each time instance t, the power demand $P_d(t)$ requested by the driver must be delivered by the engine and motor, which are the two driving power sources.

$$P_d(t) = P_m(t) + P_e(t) \tag{11}$$

where $P_m(t)$ and $P_e(t)$ are the electric motor power and mechanical engine power, respectively. The fuel power $P_f(t)$ that is assumed to be proportional to the fuel-consumption rate is expressed in terms of the associated engine power as follows:

$$P_f(t) = \frac{P_e(t) + P_0}{e}\chi(t) \tag{12}$$

where the parameter $e \in (0, 1)$ refers to the internal efficiency of fuel to mechanical power conversion in engine, P_0 denotes a friction power that is required for engine cranking, and $\chi(t) \in \{0, 1\}$ denotes the state of the engine clutch, as previously explained. As the motor serves as a generator, the battery power is expressed as follows:

$$P_b(t) = \frac{P_m(t)}{\eta^{\text{sign}(P_m(t))}} \tag{13}$$

where $\eta \in (0, 1)$ denotes the efficiency of an electric motor.

The change of battery energy over time can be expressed as the sum of the total power loss and the transmitted power. If the battery is charging, the battery power is set to a negative value. The differential equation for electrical energy of a battery denoted by E_b is given by

$$\frac{dE_b}{dt}(t) = -P_b(t) - P_\ell(P_b(t)). \tag{14}$$

Applying Taylor series expansion for linearization of (10) around a nominal battery power $P_b(t) = 0$, the dissipated power can be approximated as a quadratic function of the battery power [45]:

$$P_\ell(P_b(t)) \approx \frac{R_T(\xi(t))}{V_{oc}^2(\xi(t))}P_b^2(t) = \alpha(\xi(t))P_b^2(t) \tag{15}$$

This quadratic approximation of power dissipation is particularly useful for deriving an analytical solution of the ECMS-based operating-mode determination in Section III-B. This linearization plays a crucial role in obtaining the proposed ECMS solution and solving the associated economic hybrid MPC problem; however, it does not restrict the applicability of the minimum principle. Without the linear approximation of the power loss, numerical optimization should be performed for the minimum principle to determine the optimal control command of the motor power.

B. OPERATING CONSTRAINTS
1) BATTERY OPERATING LIMITS

In practice, the battery voltage V_b of the equivalent circuit depicted in Figure 2 is limited to a narrow band around V_{oc}, $V_b \in [V_{b,\min}, V_{b,\max}]$. In the case of discharging, the power $P_b(t)$ is positive and has a maximum power $P_b^* = V_{oc}^2/4R_T$ when $V_b^* = V_{oc}/2$ and the typical values of $V_{b,\min}$ are higher

than V_b^*. For such cases, we obtain a maximum power that can be delivered from the battery as follows:

$$P_{b,\max}(\xi(t)) = \frac{V_{oc}(\xi(t)) - V_{b,\min}}{R_T(\xi(t))} V_{b,\min} \qquad (16)$$

The corresponding limit of the discharge current is

$$I_{b,\max}(\xi(t)) = \frac{V_{oc}(\xi(t)) - V_{b,\min}}{R_T(\xi(t))} \qquad (17)$$

In the case of charging, power $P_b(t)$ is negative, and $V_b(t) > V_{oc}(\xi(t))$ and has a maximum power in absolute value that is limited by the maximum allowed battery voltage $V_{b,\max}$:

$$P_{b,\min}(\xi) = -\frac{V_{b,\max} - V_{oc}(\xi)}{R_T(\xi)} V_{b,\max} \qquad (18)$$

The corresponding limit of the charge current is

$$I_{b,\min}(\xi) = -\frac{V_{b,\max} - V_{oc}(\xi)}{R_T(\xi)} \qquad (19)$$

The constraint for operating the battery in a safe region is as follows.

$$\xi(t) \in [\xi_{\min}, \xi_{\max}] \qquad (20)$$

2) ENGINE AND MOTOR OPERATING LIMITS

In addition to battery operating limits, we should consider the physical limitations on operating the powertrain, engine and motor.

$$P_e(t) \in [0, P_{e,\max}] \text{ and } P_m(t) \in [P_{m,\min}, P_{m,\max}] \qquad (21)$$

where $P_{e,\max}$ is the maximum power that the engine can deliver to the wheel, $P_{m,\min}$ is the minimum power with negative sign that the motor can generate for charging a battery, and $P_{m,\max}$ is the maximum power that the motor can deliver to the wheel. To be more practical, the maximum and minimum power of the engine and motor are determined according to the angular speed of engine and motor. From a real vehicle test with a commercial PHEV, a set of experimental data $\{(\omega_e^i, \overline{T}_e^i)\}$ is obtained for tests of electric motor, where ω_e^i is the ith rotational engine speed and $\overline{T}_e^i$ is the corresponding measured maximum engine torque. The maximum torque and power of engine are obtained as piecewise linear functions of engine speed in the form of

$$T_{e,\max}(\omega_e) = \frac{\overline{T}_e^{i+1} - \overline{T}_e^i}{\omega_e^{i+1} - \omega_e^i} \left(\omega_e - \omega_e^i \right) + \overline{T}_e^i,$$

$$P_{e,\max}(\omega_e) = \omega_e T_{e,\max}(\omega_e)$$

for $\omega_e \in [\omega_e^i, \omega_e^{i+1}]$. The computed maximum torque curve as a function of engine speed is shown in Figure 5.[1]

Similar to the engine tests, from a real vehicle test with a commercial PHEV, a set of experimental data $\{(\omega_e^i, \underline{T}_m^i, \overline{T}_m^i)\}$ is obtained, where ω_m^i is the ith rotational motor speed, and $\underline{T}_m^i$ and $\overline{T}_m^i$ are the corresponding measured minimum and maximum motor torque, respectively. The maximum/minimum torque and power of a traction motor are
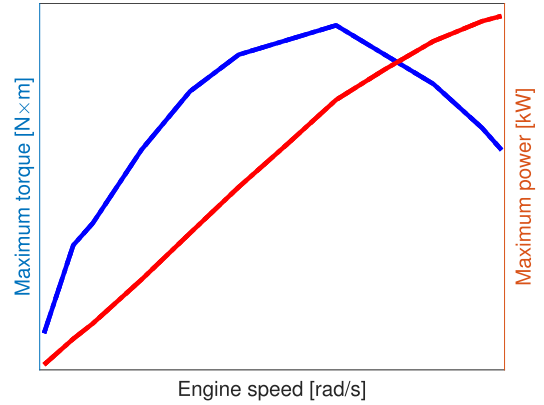

FIGURE 5. Maximum torque and power curve of the engine.

determined as piecewise linear functions of the motor speed in the form of

$$T_{m,\max}(\omega_m) = \frac{\overline{T}_m^{i+1} - \overline{T}_m^i}{\omega_m^{i+1} - \omega_m^i} \left(\omega_m - \omega_m^i \right) + \overline{T}_m^i,$$

$$P_{m,\max}(\omega_m) = \omega_m T_{m,\max}(\omega_m),$$

$$T_{m,\min}(\omega_m) = \frac{\underline{T}_m^{i+1} - \underline{T}_m^i}{\omega_m^{i+1} - \omega_m^i} \left(\omega_m - \omega_m^i \right) + \underline{T}_m^i,$$

$$P_{m,\min}(\omega_m) = \omega_m T_{m,\min}(\omega_m)$$

for $\omega_m \in [\omega_m^i, \omega_m^{i+1}]$. The computed maximum and minimum torque curve according to motor angular speed are represented in Figure 6.[1]
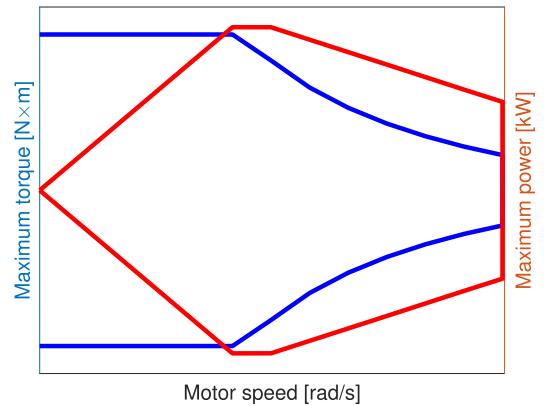

FIGURE 6. Maximum/minimum torque and power curve of the motor.

C. EMISSION MODEL

To consider the legislation of environmental pollutants, the penalty for exhaust emission such as NO_x and HC must be included in the objective function. In this article, polynomial regression functions for exhaust emission are determined based on emission map data. The regression models for NO_x and HC are selected to be the 7th-order polynomial functions

---

[1]Owing to the proprietary nature of the technical specifications of the car maker, the axis values are not specified.
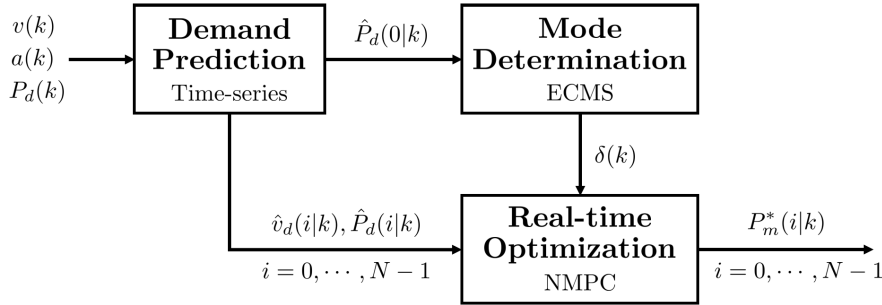
FIGURE 7. Hierarchical supervisory control architecture that consists of (i) Demand Prediction, (ii) ECMS-based Mode Determination, and (iii) NMPC-based Real-time Optimization.

for engine speed and torque:

$$\hat{f}_{\text{NO}_x}(\omega_e, T_e) = \sum_{i=1}^{7} \sum_{j=0}^{i} c_{j,i-j}\omega_e^j T_e^{i-j} \text{ [g/kWh]},$$

$$\hat{f}_{\text{HC}}(\omega_e, T_e) = \sum_{i=1}^{7} \sum_{j=0}^{i} d_{j,i-j}\omega_e^j T_e^{i-j} \text{ [g/kWh]}.$$

The associated models of the emission flow rates are represented as

$$\dot{m}_{\text{NO}_x}(t) = P_e(t) \cdot \hat{f}_{\text{NO}_x}(\omega_e(t), T_e(t)) \cdot \frac{1}{3600} \text{ [g/s]},$$

$$\dot{m}_{\text{HC}}(t) = P_e(t) \cdot \hat{f}_{\text{HC}}(\omega_e(t), T_e(t)) \cdot \frac{1}{3600} \text{ [g/s]}$$

where $\omega_e(t)$ and $T_e(t)$ are the functions of the vehicle speed $v(t)$ and engine power $P_e(t)$:

$$\omega_e(t) = \frac{\gamma_{\text{gear}(v(t))}\gamma_{\text{final}}}{r_{\text{w}}}v(t), \quad T_e(t) = \frac{r_{\text{w}}}{\gamma_{\text{gear}(v(t))}\gamma_{\text{final}}}\frac{P_e(t)}{v(t)}.$$

D. FORMULATION OF ECONOMIC OPTIMAL CONTROL PROBLEM

In this section, we propose an optimal control problem to design a supervisory controller for energy management that leads to minimum fuel consumption over a driving period $t \in [0, t_f]$. The resultant optimal control problem is defined in the form of a mixed-integer nonlinear dynamic optimization.

$$\underset{\{P_m(t), \chi(t)\}}{\text{minimize}} J = \int_{t_0}^{t_f} \frac{P_d(t) - P_m(t) + P_0}{e}\chi(t)dt$$

$$+ \int_{t_0}^{t_f} \left\{\dot{m}_{\text{NO}_x}(t) + \dot{m}_{\text{HC}}(t)\right\}dt$$

subject to

$$\frac{d\xi}{dt} = F(\xi(t), P_m(t)), \quad \xi(t_0) = \xi_0$$

$$\xi(t) \in [\xi_{\min}, \xi_{\max}]$$

$$P_m(t) \in [P_{m,\min}(\omega_m), P_{m,\max}(\omega_m)]$$

$$P_d(t) - P_m(t) \in [0, P_{e,\max}(\omega_e)]$$

$$0 \leq P_b(t) \leq P_{b,\max}(\xi(t)) \text{ for discharging}$$

$$0 \leq I_b(\xi(t), P_m(t)) \leq I_{b,\max}(\xi(t)) \text{ for discharging}$$

$$P_{b,\min}(\xi(t)) \leq P_b(t) \leq 0 \text{ for charging}$$

$$I_{b,\min}(\xi(t)) \leq I_b(\xi(t), P_m(t)) \leq 0 \text{ for charging}$$

$$\chi(t) \in \{0, 1\}$$

$$\xi(t_f) = \xi_0 \qquad (22)$$

where $I_b(\xi(t), P_m(t))$ is obtained in (7) by replacing $P_b(t)$ by $P_m(t)\eta^{-\text{sign}(P_m(t))}$. The switched dynamical system equation defined by $F(\xi(t), P_m(t))$ follows the differential equation of the battery SOC in (8) with (13). The dynamical system of the battery SOC and the power flow equations are presented in Section II-A. The operating limits of the battery, motor, and engine are presented in Section II-B. The energy management of an HEV aims at determining the power flow at each time instance among the powertrain components while satisfying these system equations and constraints. The equality state-constraint $\xi(t_f) = \xi_0$, called the *charge-sustaining* constraint, is introduced to ensure that the final battery SOC is equal to the initial value. When this condition is relaxed, it can be included in the cost function as a soft constraint rather than a hard constraint. Its explicit representation is provided and further investigated subsequently in Section III-C.

III. HIERARCHICAL SUPERVISORY CONTROL FOR ENERGY MANAGEMENT OF PARALLEL HEV

Directly solving the optimal control problem (22) is not trivial from a computational optimization perspective. This is because there are various operating modes depending on the type of operation of the engine clutch and motor. Moreover, the battery and power-flow equations are highly nonlinear, and the constraints corresponding to the operating limits are discontinuous and nonlinear. To reduce the burden of real-time computation and increase the control reliability, we propose a hierarchical supervisory control architecture depicted in Figure 7. As previously mentioned, this control architecture consists of three separate modules: (i) demand prediction, (ii) ECMS-based mode determination, and (iii) NMPC-based real-time optimization. These three modules can be designed independently and are connected in series for performing computer-aided control.

When the current time is k and the prediction horizon used in predictive control is N, the demand prediction module forecasts the power requests of the driver $\hat{P}_d(k) := [\hat{P}_d(0|k), \hat{P}_d(1|k), \cdots, \hat{P}_d(N-1|k)]^\top \in \mathbb{R}^N$ over the

prediction horizon. By abuse of notation, for a signal $x(t)$ with $t \geq 0$, we present $x(i|k) := x((k + i)t_s)$, $k \in \mathbb{Z}_+$ and $i = 0, 1, \cdots, N - 1$, where t_s is the sampling-interval.

At each time-step k, the ECMS-based mode determination module decides the operating mode $\delta(k)$ based on the current value $\hat{P}_d(0|k)$ among the forecasted power demand profile.

Based on the forecasted power demand profile $P_d(k)$ and the determined operating mode $\delta(k)$, the model-based real-time optimization module corresponding to the nonlinear MPC computes the optimal motor power $P_m^*(k) := (P_m^*(0|k), \cdots, P_m^*(N - 1|k)) \in \mathbb{R}^N$ over the prediction horizon. Then, the motor (or inverter) controller is requested to deliver the mechanical power $P_m(k) = P_m^*(0|k)$. In actual driving, on-board sensors and estimators provide feedback information of the actual vehicle speed and the battery SOC, or their changes, and the above process of computing the required motor power is repeated. This feedback control scheme is known as *receding horizon control* (RHC). The three modules of the hierarchical supervisory control architecture are further investigated in subsequent subsections.

A. DEMAND PREDICTION

For forecasting the vehicle speed and traction-power demand, we presume that both onboard sensors and vehicle-to-everything (V2X) communication are available to acquire information about the driving environment, and learn the habits and dispositions of the driver. For demand prediction, any forecasting method such as time-series, machine learning, and extrapolation could be used in principle. The forecasted power-demand can be also modeled as a Markov process to consider the uncertainty of the power-demand of the driver in various driving environments [46]. The authors of [47] used a probabilistic driving route prediction system trained using inverse reinforcement learning, and the route choice of the driver was modeled as a Markov decision process. In [48], a radial basis function neural network is developed for short-term velocity prediction. In addition, traffic-information-based trip modeling using onboard GPS and GIS to obtain a driving cycle is shown in [49]. It was conducted differently on the local road and freeway situations.

In this study, we designed a demand prediction module based on the time-series method with the autoregressive moving average (ARMA) model. When the current time is k and m pieces of previous data are used as inputs, the predicted vehicle speed $\hat{v}_d(k)$ and demand power $\hat{P}_d(k)$ can be expressed as

$$\hat{v}_d(k) = A_1 f_1(u_{1,m}(k)) + A_2 f_2(u_{2,m}(k)) + A_3 f_3(P_{d,m}(k)),$$
$$\hat{P}_d(k) = A_1 f_1(u_{1,m}(k)) + A_2 f_2(u_{2,m}(k)) + A_3 f_3(P_{d,m}(k))$$

where $A_i \in \mathbb{R}^{N \times m}$ are the coefficient matrices, $u_{i,m}(k) = [u_i(k-1) \, u_i(k-2) \cdots u_i(k-m)]^\top \in \mathbb{R}^m$ are the input vectors, $f_i : \mathbb{R}^m \to \mathbb{R}^m$ are appropriate basis functions of inputs, for $i = 1, 2, 3$, and $m \in \mathbb{N}$ is the horizon length of time lag. The input vectors $\{u_1, u_2, u_3\}$ correspond to the vehicle speed,

acceleration, and demand power, respectively. They are the the inputs to the demand prediction module in Figure 7.

In the case of real driving data, sensor-measured information such as APS, BPS, road slope can be used as input of the prediction module. However, other known driving cycles do not have sensor-measured data, so only the above three data are used for scalability of the demand prediction module. The m-dimensional vector $P_{d,m}(k) = [P_d(k - 1), P_d(k - 2), \cdots, P_d(k - m)]^\top \in \mathbb{R}^m$ is a previous power demand profile with finite memory of size m. Therefore based on the above equation, it is possible to predict a power demand profile $\hat{P}_d(k) \in \mathbb{R}^N$ for the MPC prediction horizon of N. In our case studies in Section IV, powertrain-related data such as torque and power profiles of engine and motor are obtained from on-board sensors of a real-world PHEV in driving tests. For such a case, the power-demand prediction can be directly performed with the output data $P_d = P_e + P_m$. For conventional driving cycles, the longitudinal vehicle dynamics in Section II-A1 with the pre-filtering procedure in Section IV-D1 are used for power demand prediction.

In this study, 50% of the actual driving data is used as training data, and the remaining 50% is used as test data to compare with the actual demand of traction-power. In Figure 8, the actual vehicle speed/power-demand and the forecasted vehicle speed/power-demand are compared. The normalized root-mean-square-error (RMSE) of the forecasted vehicle speed and power in test data are 0.03 % and 8.13 % after correcting time-delay in powertrain control commands and responses, respectively. This error analysis verifies that when scheduling dual-source powertrain operation, the proposed method of power-demand prediction can provide fairly accurate forecasting traction-power requests.

B. ECMS-BASED MODE DETERMINATION

In this section, we present a rule-based strategy of determining the operating powertrain mode. The mode-determination strategy is based on Pontryagin's minimum principle that gives necessary conditions for an optimal control strategy. Based on the predicted instantaneous power-demand for vehicle traction $\hat{P}_d(0|k)$ that is computed by the demand prediction module, the mode determination module in Figure 7 identifies which powertrain mode is recommended to operate over a prediction horizon of planning in the subsequent real-time optimization module.

The presented method is adopted from the results in [45] with modifications in the adaptation law for updating the co-state variable s and selecting varying parameters of the battery power-loss coefficient α, the engine efficiency e, and the friction loss of engine P_0. When there are no constraints of motor and engine in the optimal control problem (22), the Hamiltonian is expressed as (23), shown at the bottom of the next page, a piecewise function of motor power, where $H_{bo}(P_m; s, P_d)$, $H_{th}(P_m; s, P_d)$, $H_{re}(P_m; s, P_d)$, $H_{el}(P_m; s, P_d)$, $H_{el}^-(P_m; s, P_d)$ are the Hamiltonians of the *boosting*, *pure thermal operation*, *recharging*, *pure*
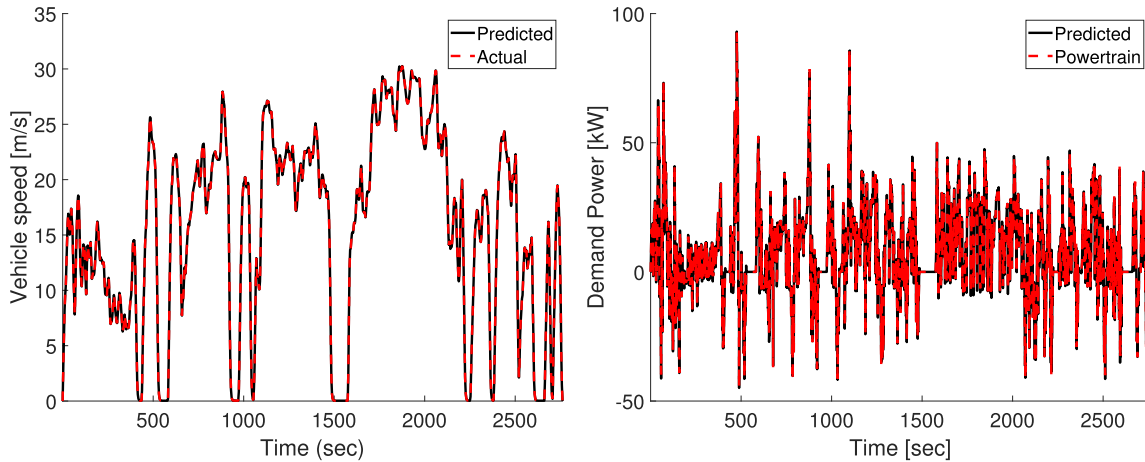
FIGURE 8. Actual vehicle speed/demand-power and forecasted vehicle speed/demand-power by applying time-series method based on the real driving data with CD-CS mode.

electric propulsion, and *pure electric recuperation* modes, respectively.

With the Hamiltonian defined in (23), and from the Pontryagin's minimum principle, the optimal control input P_m^*, the instantaneous motor power, necessarily minimizes $H(P_m; s, P_d)$ for given (s, P_d). Since $H(P_m; s, P_d)$ is piecewise continuous and differentiable for any given (s, P_d), the minimizer P_m^* can be obtained by differentiating the Hamiltonians associated with given (s, P_d) and comparing them each other in terms of the conditions on (s, P_d). To be more precise, one can rewrite the minimizer as $P_m^*(s, P_d)$. This implies that the optimal driving mode is determined by the values of s and P_d. The conditions for the five operation modes of HEV powertrain are defined in terms of the power demand P_d and equivalence factor s as the following:

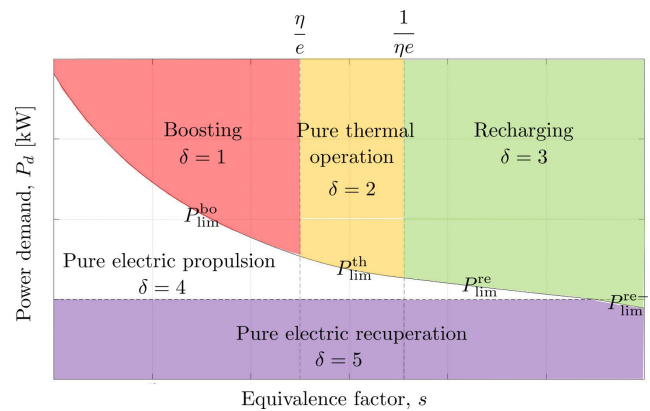**FIGURE 9.** Disjoint regions of power demand and equivalence factor for the five different operating modes of HEV powertrain.

$$
\delta(k) = \begin{cases}
1 & \text{if } (P_d > P_{\text{lim}}^{\text{bo}}(s) > 0) \bigcap (s < \frac{\eta}{e}) \\
2 & \text{if } (P_d > P_{\text{lim}}^{\text{th}}(s) > 0) \bigcap (\frac{\eta}{e} \leq s \leq \frac{1}{\eta e}) \\
3 & \text{if } \{(P_d > P_{\text{lim}}^{\text{re}}(s) > 0) \bigcap (s > \frac{1}{\eta e})\} \\
& \quad \bigcup \{(P_d < 0) \bigcap (P_d > P_{\text{lim}}^{\text{re}}(s))\} \\
4 & \text{if } (P_d < 0) \bigcup (P_d < P_{\text{lim}}^{\text{re-}}(s)) \\
5 & \text{if otherwise}
\end{cases}
$$

where the boundaries of power limits associated operating modes are defined as

$$
P_{\text{lim}}^{\text{bo}}(s) = -A + \sqrt{4BC}
$$

$$
P_{\text{lim}}^{\text{th}}(s) = \frac{1}{2B}\left(-A + \sqrt{A^2 + 4BC}\right)
$$

$$
P_{\text{lim}}^{\text{re}}(s) = \frac{1}{2B}\left(-A + \sqrt{A^2 - F^2 + 4BC}\right)
$$

$$
P_{\text{lim}}^{\text{re-}}(s) = \frac{1}{2D}\left(-E + \sqrt{4DC}\right)
$$

$$
H(P_m; s, P_d) = \begin{cases}
H_{\text{bo}}(P_m; s, P_d) = \dfrac{P_d + P_0}{e} + \left(\dfrac{s}{\eta} - \dfrac{1}{e}\right) P_m + \dfrac{s\alpha}{\eta^2} P_m^2 & \text{if } 0 < P_m < P_d \\[4mm]
H_{\text{th}}(P_m; s, P_d) = \dfrac{P_d + P_0}{e} & \text{if } P_m = 0 < P_d \\[4mm]
H_{\text{re}}(P_m; s, P_d) = \dfrac{P_d + P_0}{e} + \left(s\eta - \dfrac{1}{e}\right) P_m + s\alpha\eta^2 P_m^2 & \text{if } P_m < 0 < P_d - P_m \\[4mm]
H_{\text{el}}(P_m; s, P_d) = \dfrac{s}{\eta} P_m + \dfrac{s\alpha}{\eta^2} P_m^2 & \text{if } P_m = P_d \geq 0 \\[4mm]
H_{\text{el}}^-(P_m; s, P_d) = s\eta P_m + s\alpha\eta^2 P_m^2 & \text{if } P_m = P_d \leq 0
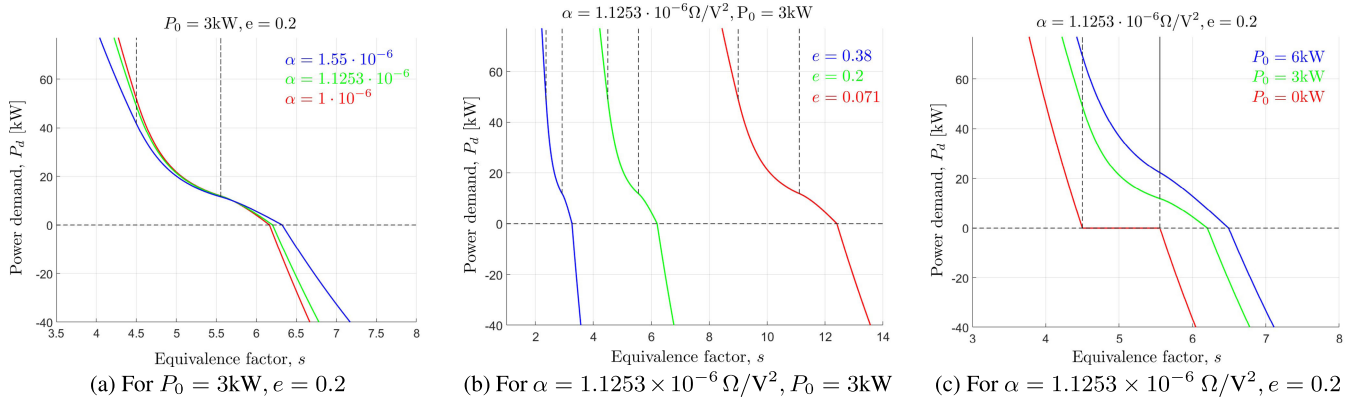\end{cases} \tag{23}
$$

FIGURE 10. The change of zones for each operating mode according to one varying parameter with the other two fixed parameters of the tuple (α, e, P_0).

with $A = (s/\eta - 1/e)$, $B = s\alpha/\eta^2$, $C = P_0/e$, $D = s\alpha\eta^2$, $E = (s\eta - 1/e)$, and $F = (s/\eta - 1/e\eta^2)$. Figure 9 shows the partitions of the (s, P_d) domain into the five powertrain operation modes of parallel HEV and the associated control variables are described in Table 2. The hyper-parameters characterizing the aforementioned rule-based ECMS algorithm for determining the driving operation modes are α, e, and P_0. Figure 9 represents the zones of operating modes when each parameter has a specific value, and the zones for each operating mode is updated based on the parameter values.

TABLE 2. Driving operation modes and the associated control variables.

Mode	$\delta(k)$	$P_m(k), P_b(k), I_b(k)$	$\chi(k)$
boosting	1	> 0	1
pure thermal operation	2	$= 0$	1
recharging	3	< 0	1
pure electric propulsion	4	> 0	0
pure electric recuperation	5	< 0	0

First, $\alpha = R_T/V_{oc}^2$ is a function of SOC and indicates the loss coefficient when approximating the power dissipation to the quadratic function of battery power (15). If the optimum motor power is determined, the SOC is updated based on equation (8). With the updated SOC, V_{oc} and R_T are obtained through the polynomial regression shown in Figure 3, and α is updated simultaneously. Figure 10 represents the change of regions for operating modes for the three different values of $\alpha = 1.55 \times 10^{-6}$ Ω/V^2, 1.1253×10^{-6} Ω/V^2, 1×10^{-6} Ω/V^2. These values are carefully chosen to make the rule-based operating mode determination to be state-dependent so that the charge-sustaining capability can be further improved without knowing the future driving conditions. This is another difference from the existing ECMS-based strategies of the supervisory control for HEVs.

Second, if the power required to be generated by the engine is determined when the demand power is given, the engine operates according to the engine optimal operating line based on the brake specific fuel consumption (BSFC) data. The

engine speed and torque can be obtained from the operating point determined by the operating line. Therefore, the engine efficiency e is updated based on the engine efficiency map at the operating point. When the engine efficiency is $e = 0.071$, 0.2, 0.38, the change of zones for operating mode is shown in Figure 10b.

Lastly, P_0 is the friction loss of engine which is dependent on engine speed. In general, it is difficult to measure and is assumed to be used as a constant. In this study, two values (P_0^{on}, P_0^{off}) are used for friction loss in consideration of the coefficient of kinetic friction and static friction. The friction loss is expressed as P_0^{on} due to the kinetic friction coefficient when the engine state goes from $\chi = 0$ to $\chi = 1$. In addition, when the engine state was continuously $\chi = 1$ or switching from $\chi = 1$ to $\chi = 0$, the friction loss due to the static friction coefficient is expressed as P_0^{off}, and P_0^{on} has a larger value than P_0^{off}, i.e., $P_0^{\text{on}} \leq P_0^{\text{off}}$. Thus, it is possible to reduce the frequency of transition of the engine state and the transient phenomenon that occurs when switching from $\chi = 0$ to $\chi = 1$ by setting the engine friction appropriately. Figure 10c shows the change of zones for operating modes when $P_0 = 0\,\text{kW}$, $3\,\text{kW}$, and $6\,\text{kW}$. Based on these numerical experiments, we use the values of $P_0^{\text{on}} = 6$ kW and $P_0^{\text{off}} = 4.2$ kW. Moreover, the parameters necessary for the rule-based algorithm are not fixed but are set adaptively to be state-dependent.

The co-state is updated via the following law of adaptation to the current level of battery SOC:

$$s(k+1) = s(k) + K_p \Delta\xi(k) + K_i t_s \sum_{i=1}^{k} \Delta\xi(i) \quad (24)$$

where $\Delta\xi(k) = \xi_{\text{ref}}(k) - \xi(k)$ is the deviation of the state of charge from the reference value at time-step k. The variables $s(k)$ and $\xi(k)$ are the co-state and battery SOC at time-step k, respectively. Appropriate values of the tuning parameters K_p and K_i can be determined only given the driving cycle. In general, they can be found only when a driving cycle is given. In this study, they are set as Table 4 based on numerous numerical simulations.

C. ECONOMIC NONLINEAR MODEL PREDICTIVE CONTROL

The NMPC-based real-time optimization module defines a nonlinear predictive control problem using a practical model of the physical system such as the battery, engine, and motor. The goal of NMPC is to optimize fuel efficiency, keep battery SOC adequate, and reduce emissions to exhaust emissions. The purpose of the nonlinear predictive control problem is to optimize fuel efficiency, which is the goal of the original optimal control problem, as well as to maintain battery SOC properly. Therefore, the hard constraint in (22) was converted into a soft constraint by using the battery charge sustaining parameter $q_{\delta(i|k)}$. As a weight for the proper adaptation of the fuel usage and battery usage, the battery charge sustaining parameter was multiplied by the battery usage. The unit of cost function is then set as energy by multiplying the fuel usage part by the sampling time t_s and the battery use part by $Q_{nom}V_{oc}$. In addition, to consider the regulation of environmental pollutants, the penalty for exhaust emission such as NO_x and HC was included in the objective function. The unit of fuel and battery usage is J or kWh, and the unit for NO_x and HC usage is g. Therefore, in order to unify the meaning of multi-objective for NMPC, q_{NO_x} and q_{HC} were multiplied by the NO_x or HC usage.

The model predictive control problem reformulating the optimal control problem given in (22) is expressed in (25).

$$
\underset{\{P_m(\cdot|k)\}}{\text{minimize}} \sum_{i=0}^{N-1} \left| \frac{\hat{P}_d(i|k)v(\delta(k)) - P_m(i|k) + P_0}{e(k)} \right| t_s
$$

$$
+ \sum_{i=1}^{N} \left| q_{\delta(k)} \cdot Q_{nom}V_{oc} \cdot (\xi_{ref}(k) - \xi(i|k)) \right|
$$

$$
+ \sum_{i=1}^{N} t_s \left(\dot{m}_{NO_x}(i|k)q_{NO_x} + \dot{m}_{HC}(i|k)q_{HC} \right)
$$

subject to

$$
\xi(i+1|k) = F^d(\xi(i|k), P_m(i|k))
$$
$$
\xi(i|k) \in [\xi_{min}, \xi_{max}]
$$
$$
\xi(k|k) = \xi(k)
$$
$$
\max \left\{ P_{m,min}(\omega_m), \hat{P}_d(i|k) - P_{e,max}(\omega_e) \right\} \leq P_m(i|k)
$$
$$
P_m(i|k) \leq \min \left\{ P_{m,max}(\omega_m), \hat{P}_d(i|k) \right\}
$$
$$
0 \leq P_m(i|k) \leq \eta \cdot P_{b,max}(\xi(i|k)) \quad \text{for discharging}
$$
$$
P_{b,min}(\xi(i|k))/\eta \leq P_m(i|k) \leq 0 \quad \text{for charging} \quad (25)
$$

where all constraints must be satisfied for all time indices $i = 0, 1, \cdots, N-1$. The decision variables are $P_m(\cdot|k) = (P_m(0|k), P_m(1|k), \cdots, P_m(N-1|k))$ and the constraint on the battery current (17) and (19) is omitted because the operating limits on the battery power are precisely the same as the operating limits on the battery current. The driveline mode is assumed to be fixed within the prediction horizon of the MPC, and we update the engine efficiency $e(k)$ and motor efficiency $\eta(k)$ by following the regression model which is described in Section IV-B. A time-discretized state

transition equation $F^d(\xi(i|k), P_m(i|k))$ corresponding to the continuous-time SOC dynamics (8) is defined in (26) by following the fourth-order Runge–Kutta method to obtain an accurate prediction model:

$$
\xi(i+1|k) = F^d(\xi(i|k), P_m(i|k))
$$
$$
= \xi(i|k) + \frac{t_s}{6}(K_1 + 2K_2 + 2K_3 + K_4) \quad (26)
$$

where the coefficients are

$$
K_1 = F(\xi(i|k), P_m(i|k)),
$$
$$
K_2 = F\left(\xi(i|k) + \frac{t_s}{2}K_1, P_m(i|k) \right),
$$
$$
K_3 = F\left(\xi(i|k) + \frac{t_s}{2}K_2, P_m(i|k) \right),
$$
$$
K_4 = F(\xi(i|k) + t_sK_3, P_m(i|k)).
$$

Moreover, considering that the motor does not operate in pure thermal operation mode, we used the variable $v(\delta(k))$.

$$
v(\delta(k)) = \begin{cases} 1 & \text{if } \delta(k) \in \{1, 3, 4, 5\} \\ 0 & \text{if } \delta(k) \in \{2\} \end{cases}
$$

The overall flowchart of the proposed hierarchical supervisory control algorithm is shown in Figure 11.

IV. ILLUSTRATIVE CASE STUDIES

A. SIMULATION SETUP

To solve the NMPC problem involving nonlinear constraints (25), we use the built-in function `fmincon` in MATLAB. The specifications of the computer for the simulation are as follows: Intel Core (TM) i5-7400 CPU Quad Core 3.00 GHz; RAM 8.00 GB. The specific parameter values that are necessary for the optimization are divided into the system and the optimal control parameters. The parameters related with the mode-determination module, P_0^{on} and P_0^{off} are chosen to be the values given in Figure 10c. Other system parameters listed in Table 3 are selected from the actual specifications of a commercial PHEV.

TABLE 3. System parameter values used in the simulation.

Parameter	Value	Unit
P_0^{on}	6000	W
P_0^{off}	4200	W
Q_{nom}	88920	A·sec
$P_{m,min}$	−44500	W
$P_{m,max}$	44500	W
$P_{e,max}$	77000	W
$\omega_{e,max}$	596.8	rad/sec
$\omega_{m,max}$	628.3	rad/sec

The parameters of adaptive ECMS, s_0, K_p, and K_i, are selected as appropriate values based on the given driving cycle. The battery charge sustaining parameter $q_{\delta(k)}$ should be set considering the different purposes of each operating mode. For example, the pure thermal operation mode operates the engine only, and the pure electric propulsion mode operates so that the motor power is equal to the demand power.
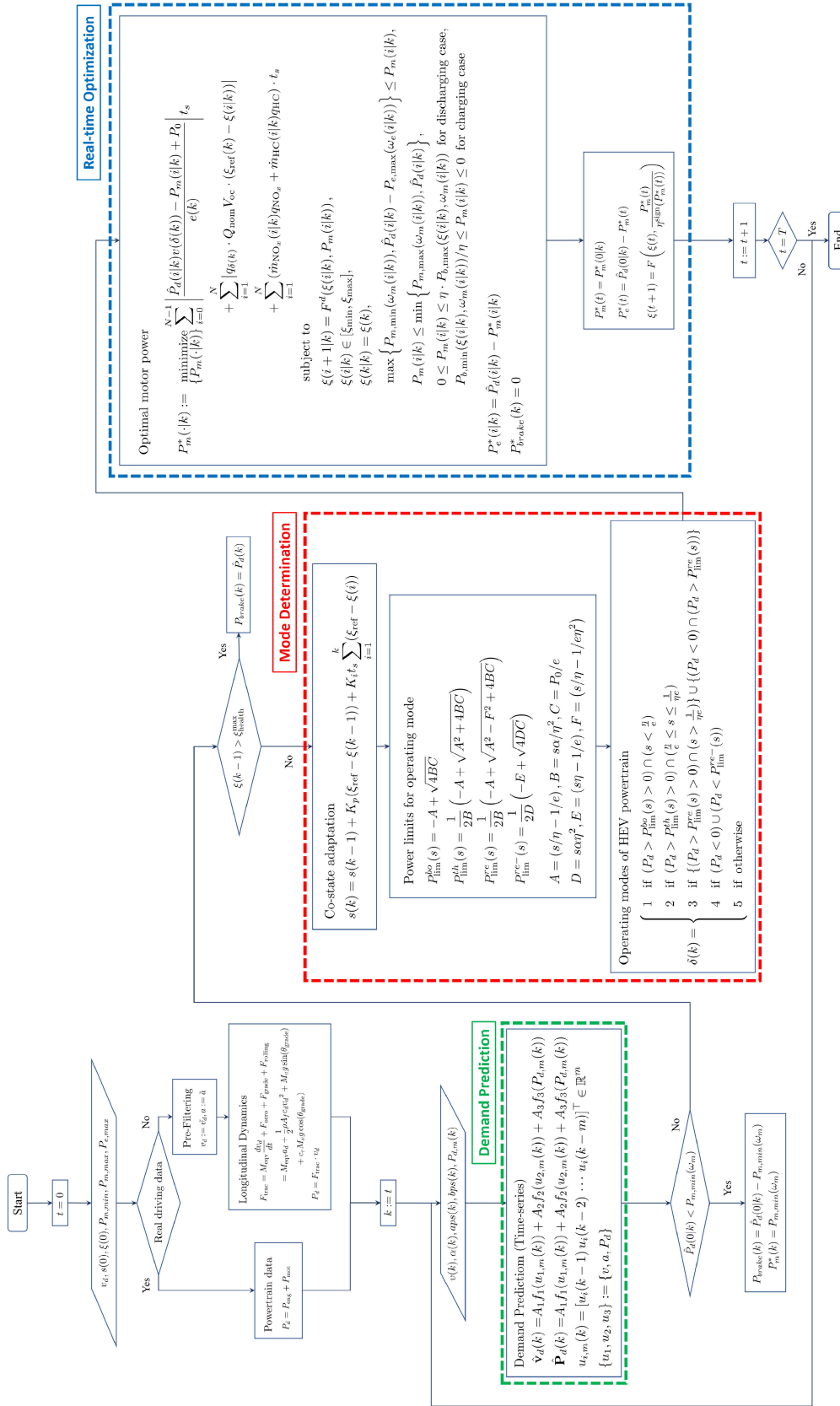
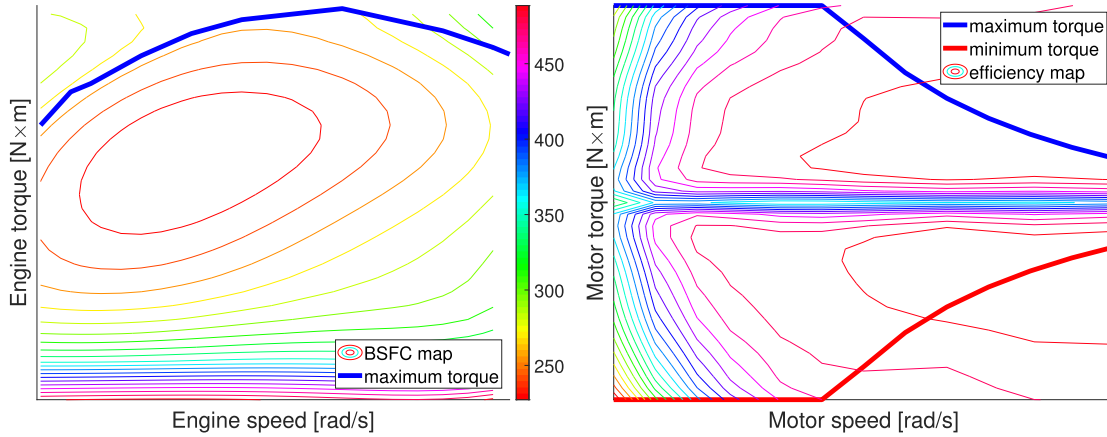**FIGURE 11.** The flow chart for the proposed hierarchical supervisory control method.

FIGURE 12. BSFC contour map (left) and motor efficiency contour map (right) based on the regression model.

TABLE 4. Optimal control parameter values used in the NMPC simulation.

Parameter	Value	Unit
s_0	5.55	-
N	5	-
K_p	1×10^{-4}	-
K_i	8×10^{-9}	-
ξ_{ref}	0.4759	-
$q_{\delta(k) \in \{1,5\}}$	10^{-3}	-
$q_{\delta(k) \in \{3\}}$	3×10^{-2}	-
$q_{\delta(k) \in \{2,4\}}$	0	-
q_{NO_x}	1	-
q_{HC}	1	-

Therefore, the battery charge sustaining parameter was set to 0 for the above two modes because it is not necessary to consider maintaining the SOC. In addition, as the battery needs to be charged in the recharging mode, the battery charge sustaining parameter should be set to a relatively large value compared to other modes. The numerical values of the optimal control hyper-parameters are given in Table 4.

B. FUEL CONSUMPTION CALCULATION

To evaluate the performance of the proposed method, the fuel economy calculation was performed using the look-up table of BSFC map for a commercial PHEV. BSFC is a value obtained by dividing the fuel mass flow by engine output power to evaluate the engine efficiency.

$$\text{BSFC} = \frac{\dot{m}_f}{P_e} 3600 = \frac{\dot{m}_f}{w_e \cdot T_e} 3600 \ [\text{g/kWh}]$$

Depending on the speed index and torque index of engine, the BSFC is usually provided in the form of map data. In this article, the regression model for BSFC was designed as a polynomial function according to speed and torque based on the BSFC map of a commercial PHEV. The order of regression is set to five, considering that the normalized RMSE of BSFC is 2.5 %.

$$\text{BSFC}(\omega_e, T_e) = \sum_{i=1}^{5} \sum_{j=0}^{i} e_{j,i-j} \omega_e^j T_e^{i-j} \ [\text{g/kWh}]$$

Once the BSFC is determined by regression model, the engine efficiency can be computed as the following:

$$e = \frac{1}{\text{BSFC} \cdot Q_{\text{lhv}}}$$

where $Q_{\text{lhv}} = 0.012069[\text{kWh/g}]$ is the specific lower heating value of gasoline. The BSFC contour map based on regression model is represented in Figure 12.[1] At this time, the engine and motor speed is determined by the transmission gear ratio according to the desired speed. The engine torque is obtained by dividing the engine power determined by our hierarchical supervisory control algorithm into speed.

In addition, the operation of motor is divided into the conditions when the motor torque is greater than zero and when it is smaller than zero, so that the motor operates in traction mode and regenerative braking mode, respectively. Likewise engine efficiency, the motor efficiency is given in the form of map data according to the speed index and torque index of motor. In this article, the regression model for motor efficiency was designed as a polynomial function according to speed and torque based on the motor efficiency map of a commercial PHEV.

$$\eta(\omega_m, T_m) = \sum_{i=1}^{6} \sum_{j=0}^{i} f_{j,i-j} \omega_m^j T_m^{i-j}$$

The order of regression is set to five, considering that the normalized RMSE of motor efficiency is 1.05 %. The motor efficiency contour map based on regression model is also represented in Figure 12.[1]

C. COMPARISONS WITH DP AND ECMS SOLUTIONS

In this section, validation of our method through numerical simulations based on actual-vehicle driving data from a commercial PHEV is presented. To compare the performance of our hierarchical supervisory control algorithm, the results of using DP or ECMS only as a control method are also provided.

TABLE 5. A comparison of fuel economy resultant from different control strategies in real driving data with CS mode.

Control method	Fuel Economy [km/l]	$SOC(t_f)$
Real driving	19.7569	0.1520
DP	20.7605	0.1198
ECMS only	19.8252	0.0820
Proposed method	20.1027	0.1133

TABLE 6. A comparison of fuel economy resultant from different control strategies in real driving data with CD-CS mode.

Control method	Fuel Economy [km/l]	$SOC(t_f)$
Real driving	23.4353	0.1500
DP	24.6330	0.1183
ECMS only	23.6124	0.0835
Proposed method	23.5680	0.1174

Tables 5 and 6 present the fuel economy calculated from the fuel economy measurement method described in Section IV-B for real driving data with CD-CS mode and CS mode, respectively.

1) DYNAMIC PROGRAMMING

The DP results are used to assess the performance of the proposed hierarchical optimal control method, as the DP solution is globally optimal. DP is a direct discrete-time method based on the principle of optimality. It employs backward iteration, which starts from the final step and proceeds backward using sequential control and generates the optimal cost-to-go function referred to as value function. The advantage of DP is that the optimal policy can be obtained even with nonlinear constraints, and the global optimality is guaranteed.

Since DP is an off-line optimization method calculated through backward induction, it is necessary to know the whole power demand of the driving cycle. In addition, we should discretize the entire possible state and input appropriately. However, if the discretized size is too small, the phenomenon of the curse of dimensionality may occur. For the numerical case studies in this article, the state variable ξ is discretized by 0.025 to $\xi_{\min}$ from $\xi_{\max}$ and the control input P_m is discretized by 1 W to $P_{m,\min}$ from $P_{m,\max}$ evenly. If we use a smaller discretized step for higher accuracy, the longer computation time would result. The engine efficiency e_k is updated by the BSFC regression model which is described in Section IV-B.

The discrete DP is formulated with the following sets of state and input variables:

$$\xi_k \in \mathbb{Q}_x = \{\xi^1, \xi^2, \cdots, \xi^{n_x}\},$$
$$P_{m,k}(\omega_{m,k}) \in \mathbb{Q}_u = \{P_{m,k}^1, P_{m,k}^2, \cdots, P_{m,k}^{n_u}\}.$$

We define the value function as follows:

$$V_N(\xi_N) := \begin{cases} \phi(\xi_N) & \text{if } \xi_N \in \mathbb{X}_N \\ \infty & \text{otherwise} \end{cases}$$

Then, the value function at k stage $V_k(\xi_k)$ is the solution of the optimization problem below.

$$\underset{\{P_{m,k}, \chi_k\}}{\text{minimize}} \left(\frac{P_{d,k} - P_{m,k} + P_0}{e_k} \chi_k \right) t_s$$
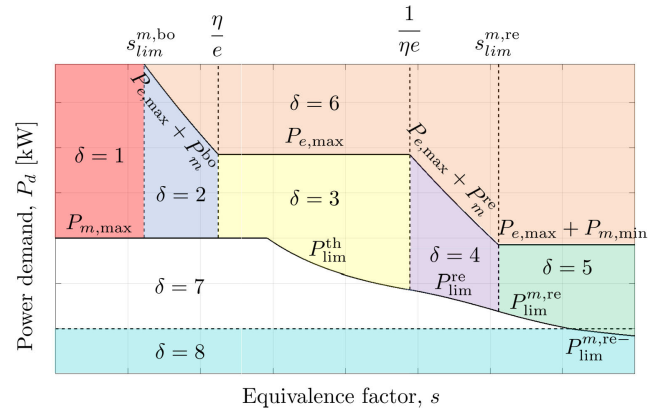

FIGURE 13. Partitions of the domain of power demand and equivalence factor for different operating modes considering engine and motor constraints.

$$+ \left\{ \dot{m}_{NO_x}(P_{m,k})q_{NO_x} + \dot{m}_{HC}(P_{m,k})q_{HC} \right\} t_s$$
$$+ q_{DP}Q_{nom}V_{oc}(\xi_k)|(\xi_{ref} - \xi_k)| + V_{k+1}(\xi_{k+1})$$

subject to

$$\xi_{k+1} = (q_k \circ f_k)(\xi_k, P_{m,k})$$
$$\xi_{k+1} \in [\xi_{\min}, \xi_{\max}]$$
$$\max\left\{P_{m,\min}(\omega_m), P_{d,k} - P_{e,\max}(\omega_e)\right\} \leq P_{m,k}$$
$$P_{m,k} \leq \min\left\{P_{m,\max}(\omega_m), P_{d,k}\right\}$$
$$\chi_k \in \{0, 1\} \tag{27}$$

where the recursion k proceeds from $N - 1$ to 0 backward, the function $q_k : [0, 1] \to \mathbb{Q}_x$ is the state-quantization map with a user-defined resolution of discretization, χ is a switching variable which indicates the engine clutch, and ϕ denotes the penalty function of terminal state. The weighting parameter of emission q_{NO_x} and q_{HC} was set the same as the value used in the NMPC simulation. In addition, the battery operation is highly dependent on battery charge sustaining parameter q_{DP}, and it was set to 4×10^{-4}, which is an appropriate value through numerical experiments.

The value table of discrete DP for optimal control problem is computed to obtain the optimal motor power of each discretized state at every stage. Therefore, the optimal trajectory can be obtained in any initial or current state of battery SOC.

2) ECMS

The application of only ECMS is similar to the description in Section III-B; however, a difference is that the engine and motor constraints (20) are considered. Therefore, the operating mode in which three modes due to constraints are added to Figure 9 is represented in Figure 13. The equations for the equivalence factor limits $s_{\lim}^{m,bo}$ and $s_{\lim}^{m,re}$ are as follows [45]:

$$s_{\lim}^{m,bo} \triangleq \frac{\eta^2}{e(2\alpha P_{m,\max} + \eta)}$$

$$s_{\lim}^{m,re} \triangleq \frac{1}{\eta e(1 + 2\alpha\eta P_{m,\min})}$$

In addition, the engine efficiency e and motor efficiency η was fixed to 0.2 and 0.9 respectively. The co-state was set to 5.65 through numerical simulations. The solution of ECMS is a simple closed-form and an open-loop system without feedback. As a result, the computational burden is extremely low, and the computation time required for the simulation was approximately 10 s.

However, it is not possible to consider limitations on the maximum torque of the engine and motor described in Section II-B, as well as the constraints on SOC to operate in a safe region (20). If the engine torque exceeds the maximum torque $T_{e,\max}(\omega_e)$ according to the engine speed, the value of BSFC and emission (NOx, HC) which is generated by the regression model are not ideal. In addition, if the motor torque exceeds the maximum torque according to the motor speed, the value of the motor efficiency obtained by the regression model is not ideal. As a result, as shown in Figure 17, the battery SOC in real driving with CS mode becomes smaller than $\xi_{\min}$ in time intervals [1030 s, 1165 s] and [1338 s, 1670 s]. In addition, the battery SOC in real driving with CD-CS mode becomes smaller than $\xi_{\min}$ after time 2313 s. This leads to excessive discharge of the battery, and thus has a serious impact on the stable operation of the battery.

D. CASE STUDIES

This section describes a case study with real driving data obtained from a commercial PHEV and well-known driving cycle such as HWFET and FTP-75 to demonstrate effectiveness and fuel economy offered by the proposed hierarchical supervisory control algorithm. In the case of real driving data, there are cases in which the initial SOC is set as small as 0.1690 to operate only in CS mode like HEV operation, and the case in which the initial SOC is set as 0.3040 to show CD-CS mode.

1) PRE-FILTERING OF REAL DRIVING DATA

As input data of demand prediction module, previous power-demand profile is needed. For real driving data, the power used in powertrain (enigne and motor) is measured from the sensor, so it can be used as the previous power-demand profile without consideration of longitudinal dynamics. However, known driving cycles do not have powertrain data, so previous demand-power must be obtained through longitudinal dynamics. This section compares the powertrain data for real driving of a commercial PHEV with demand-power obtained by longitudinal dynamics (1).

The actual speed and required acceleration are shown by the blue dashed line in Figure 14 and 15. The reason why the required acceleration is heavily noisy is that the noise component included in the measured driving speed is differentiated. Therefore, a pre-filtering process is required to remove these noise components, and we designed based on the Kalman filter. The pre-filtered acceleration represented by the red line in Figure 15 shows a similar tendency to the calculated acceleration from the measured vehicle speed. In addition, the re-calculated speed from the pre-filtered acceleration is
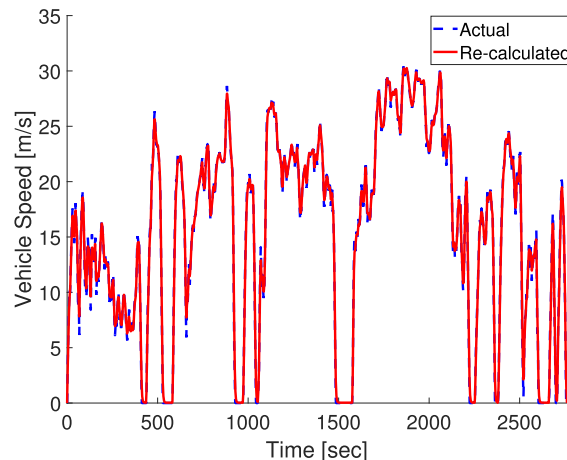

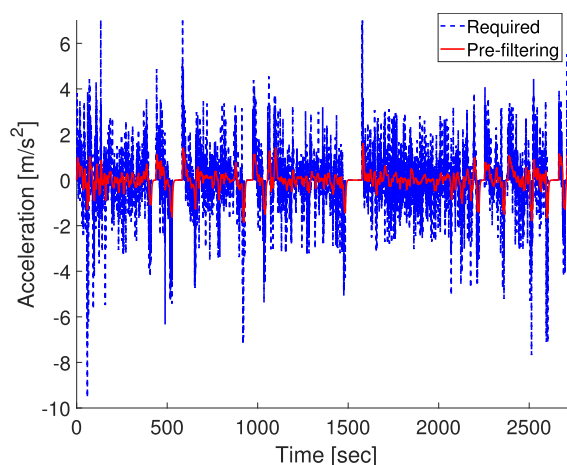**FIGURE 14.** Actual vehicle speed and re-calculated speed from pre-filtered acceleration.

FIGURE 15. Required acceleration from measured speed and pre-filtered acceleration.

the same as the blue dashed line in Figure 14, which verifies the validity of the pre-filtered acceleration.

The power obtained by applying the pre-filtered acceleration and actual vehicle speed to the longitudinal dynamics is shown as the red line in Figure 16. The difference of power occurs due to the loss of powertrain and the inaccuracy of the model caused by not considering tire dynamics or lateral dynamics in longitudinal dynamics of vehicle. Unlike known driving cycles such as HWFTP and FTP-75, real driving data has powertrain (engine and motor) data measured from the sensor, so it has the advantage of verifying the validity of power determined from longitudinal dynamics.

2) REAL DRIVING DATA WITH CS MODE

When the initial SOC is 0.1690, the commercial PHEV operates in CS mode due to the characteristics of the vehicle as shown in Figure 17. The fuel economy of actual driving data is 19.7569 and the SOC at terminal time is 0.1520, which is similar to the operation of a hybrid electric vehicle. In addition, the battery SOCs for different control strategies
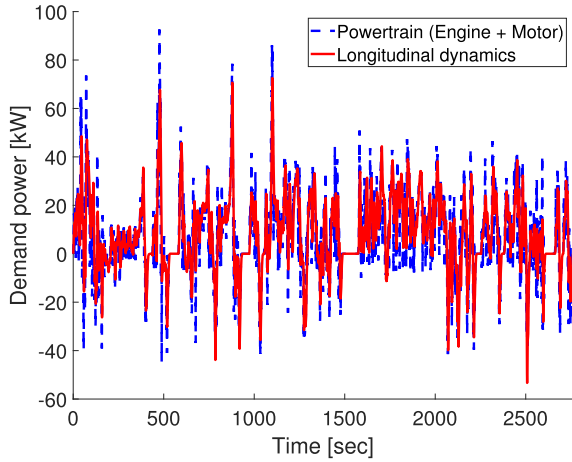
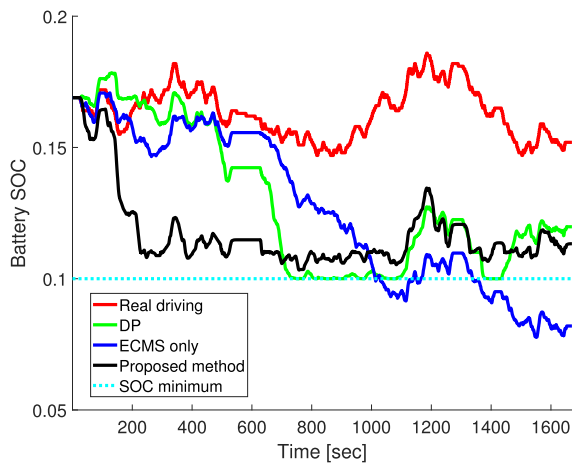**FIGURE 16.** Demand power from powertrain data and longitudinal dynamics.

FIGURE 17. A comparison of the SOC determined by control strategies based on real driving data with CS mode.

FIGURE 18. Changes of operating mode determined by the proposed method based on real driving data with CS mode.

FIGURE 19. Changes of the associated co-state determined by the proposed method based on real driving data with CS mode.

TABLE 7. Comparison of NO_x and HC emissions for different control strategies based on real driving data with CS mode.

Control method	Total NO_x [g]	Average NO_x [g/km]
Real driving	61.3486	2.0602
DP	41.9667	1.4093
ECMS only	17.9606	0.6032
Proposed method	41.1101	1.3806

Control method	Total HC [g]	Average HC [g/km]
Real driving	20.3008	0.6817
DP	19.2769	0.6474
ECMS only	18.2261	0.6121
Proposed method	19.9728	0.6707

are shown in Figure 17. The initial SOC of different control strategies was set to 0.1690, which is the same as the actual vehicle.

First, in the case of the ECMS only, the constraint on SOC is not considered, so the battery is operated in an unstable area after 1000 s. As a result, the SOC at the terminal time is 0.0820, which is smaller than the lower bound ξ_{min}. Second, in the case of DP, the SOC varies greatly depending on q_{DP}, and it was set to 4×10^{-4} through numerical experiments. At this time, SOC is equal to ξ_{min} in time intervals [750 s, 1080 s] and [1380 s, 1430 s], which means that q_{DP} needs to be adjusted more precisely in order to operate the battery in a safe area. Lastly, in the case of the proposed method, it can be seen that the tendency is similar to actual driving data, except that the overall SOC operation is performed in a low area due to large discharge in the time interval [0 s, 200 s].

The change of operating mode and co-state determined by the proposed method are shown in Figure 18 and 19. Since the SOC becomes very low after about 240 seconds, the operation mode mainly stays in the recharging mode except for the
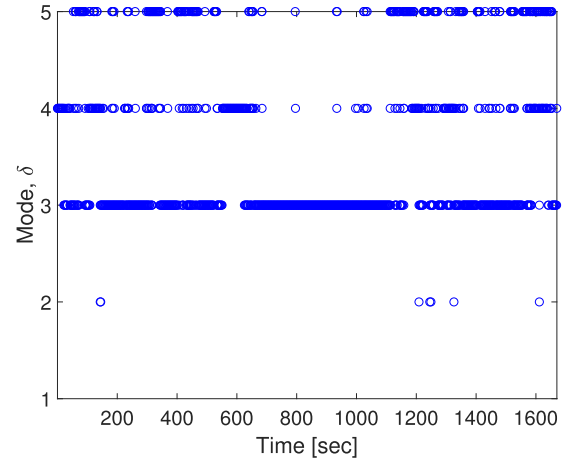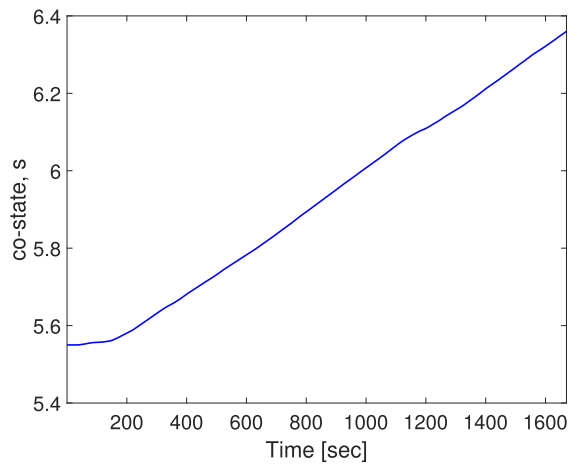
conversion to pure electric propulsion mode or pure electric recuperation mode according to demand power and co-state values. The ECMS-based mode determination module of our hierarchical supervisory control algorithm is updated based on the PI controller, as represented in equation (24). By properly setting s_0, K_p, and K_i, the co-state is changed smoothly and the frequency of converting operating modes is also reduced.

Figure 20 shows the results of forecasted power, motor and engine powers determined by the proposed method. In order
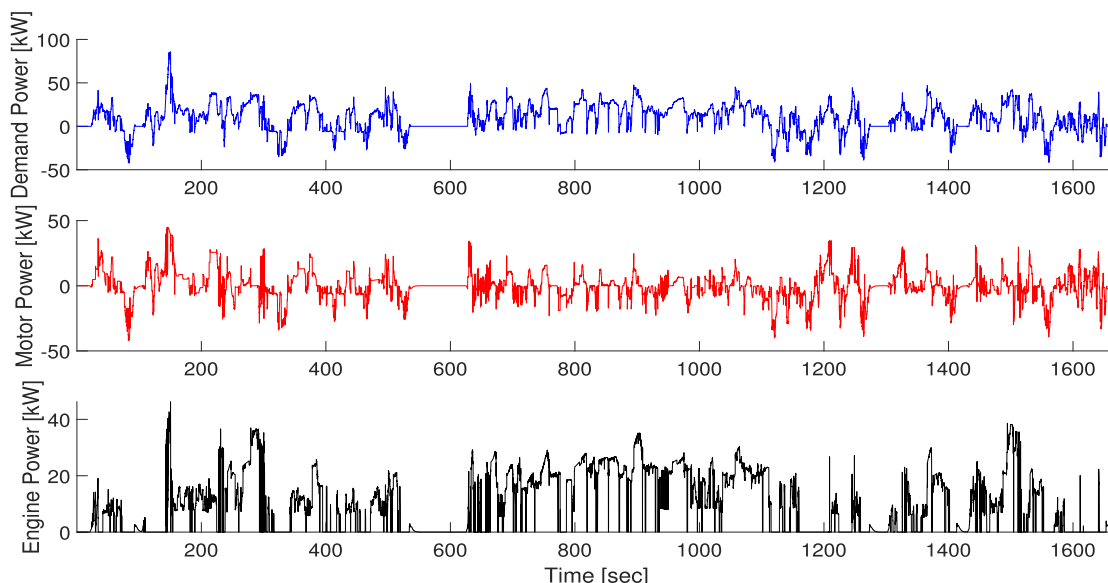
FIGURE 20. Time-series based forecasted demand, engine and motor power obtained by using the proposed method based on the real driving data with CS mode.
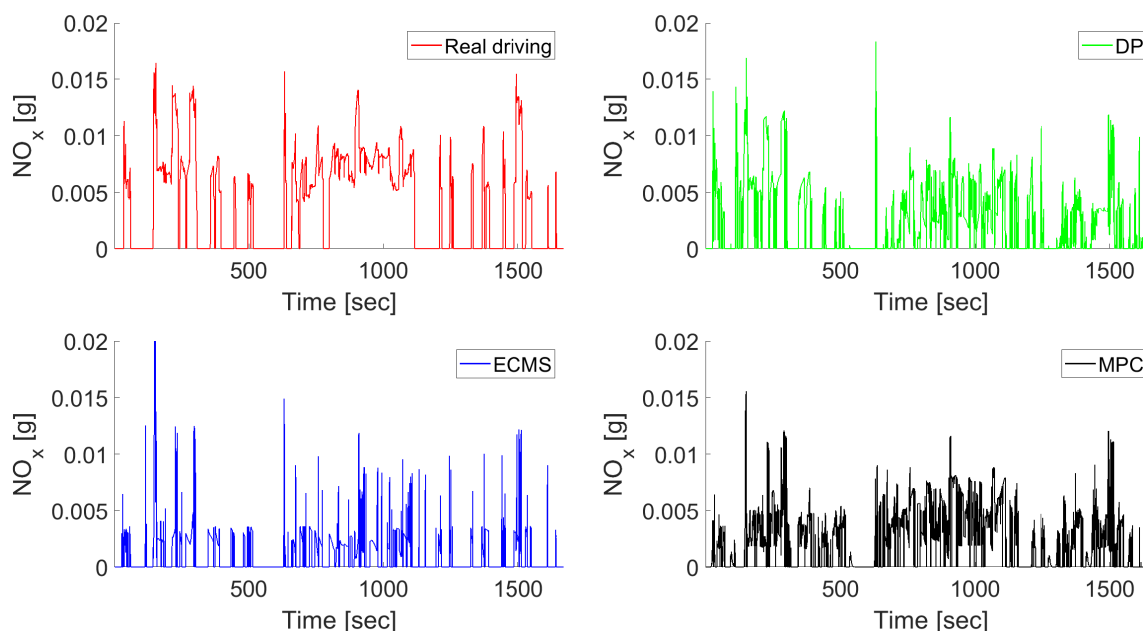

FIGURE 21. A comparison of NO_x emissions determined by control strategies based on real driving data with CS mode.

to operate the battery in a stable area, the engine mainly operates. Moreover, the engine efficiency modeled through the regression function is reflected in real time to the optimization problem so that the engine can operate at a point of high efficiency when it is operated once. As a result, the frequency of transition of engine state and transient phenomenon that occurs when switching from the $\chi = 0$ to $\chi = 1$ is quite reduced.

Based on real driving data with CS mode, the results of NO_x and HC emissions according to the control strategies are shown in Figure 21 and 22, respectively. Table 7 compares NO_x and HC emissions for different supervisory control

strategies. For real driving data, it was estimated by applying regression model described in Section II-C based on the actual speed and torque of engine. The ECMS-only method shows the lowest NO_x and HC emissions. This is because the ECMS-only results in charge-depletion beyond the minimum operation limit, which could degrade the battery performance and life. Compared to the DP solution, the proposed control strategy shows 2.04 % improvement in NO_x emission and 3.60 % degradation in HC emission. Moreover, compared to the real data, the propose method results in 32.99 % improvement in NO_x emission and 1.61 % improvement in HC emission.
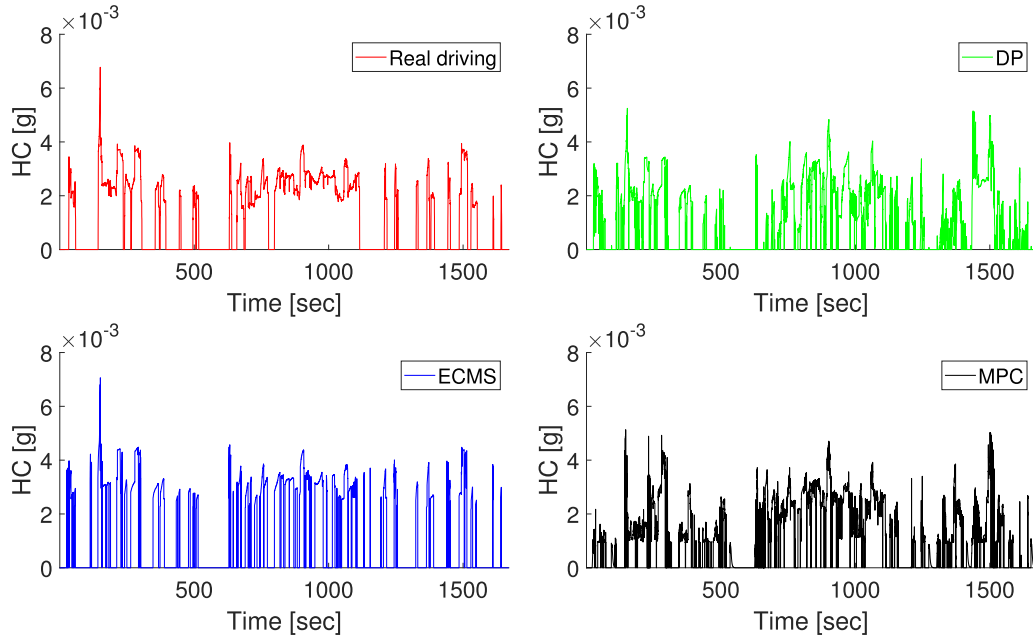
FIGURE 22. A comparison of HC emissions determined by control strategies based on real driving data with CS mode.
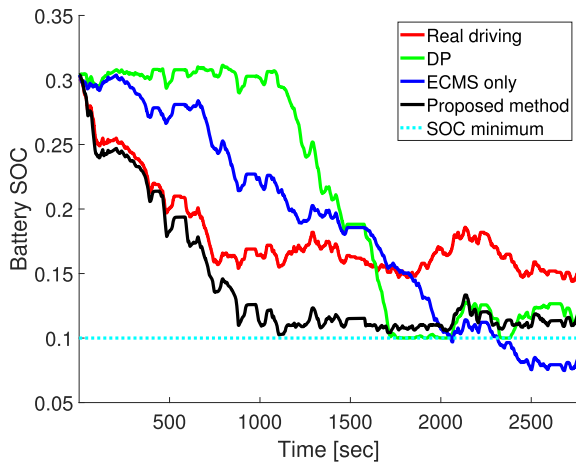

FIGURE 23. A comparison of the battery SOC determined by control strategies based on real driving data with CD-CS mode.
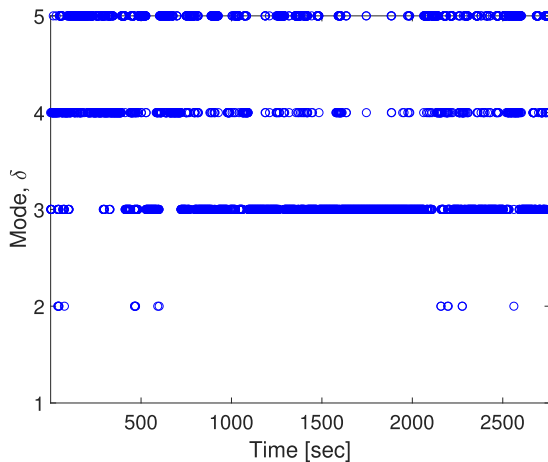

FIGURE 24. Changes of operating mode determined by the proposed method based on real driving data with CD-CS mode.
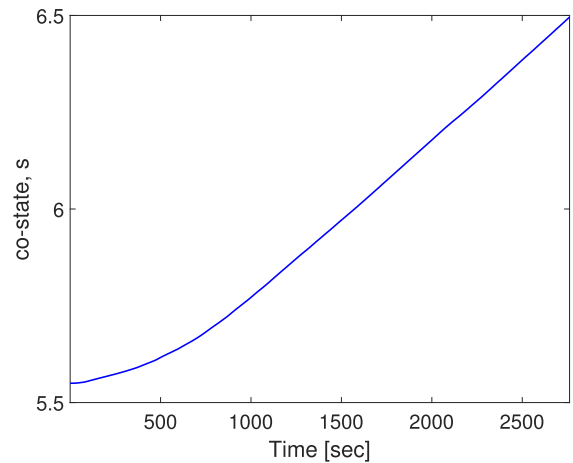

FIGURE 25. Changes of the associated co-state determined by the proposed method based on real driving data with CD-CS mode.

3) REAL DRIVING DATA WITH CD-CS MODE

Similar to the simulation of real driving data with CS mode which is described above, this section presents the verification of the effectiveness of the proposed method by comparing the simulation results obtained by DP and ECMS. First, the battery SOCs for different control strategies are as shown in Figure 23. The initial value of SOC for different control strategies was set to 0.3040, which is the same as the actual vehicle.

The SOC behavior of real driving data and the proposed method are almost the same up to 460 seconds, but the variations of SOC afterwards are significantly different depending on how much the motor is used for $460 \sim 490$ seconds. After 1000 seconds, the engine mainly operates and the motor
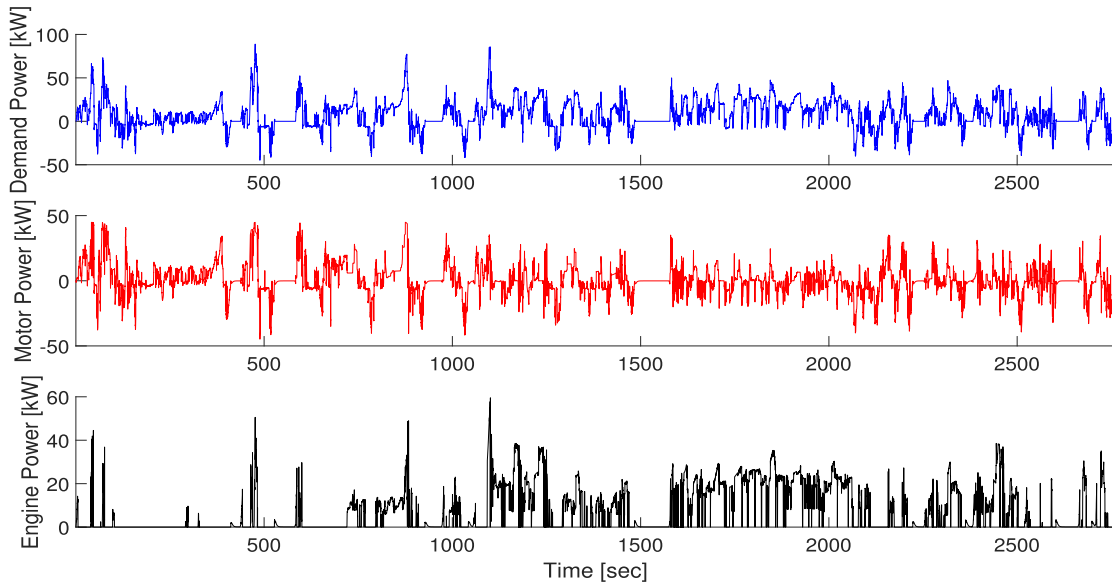
FIGURE 26. Time-series based forecasted demand, engine and motor power obtained by using the proposed method based on the real driving data with CD-CS mode.

charges the SOC slightly through regenerative braking so that it does not lower to ξ_{ref}. The NMPC-based real-time optimization module of our hierarchical supervisory control algorithm contains a soft constraint for battery usage to the cost function; hence, the battery SOC at the final time has a larger value than the lower bound ξ_{min}. It is possible to operate the battery in a safe region and attain our goals via appropriate setting of the optimal control parameters of the NMPC. As the ECMS only cannot consider the constraints, the SOC becomes lower than ξ_{min} after 2310 seconds. In the case of DP, as all information on the entire driving cycle is known, the motor and engine are appropriately used for 1700 sec, and the SOC value at the final time varies heavily depending on the battery charge sustaining parameter, q_{DP}. At this time, SOC is equal to ξ_{min} in time intervals [1750 s, 2050 s] and [2330 s, 2385 s], which means that q_{DP} needs to be adjusted more precisely in order to operate the battery in a safe area.

The change of operating mode and co-state determined by the proposed method are shown in Figure 24 and 25. Unlike the ECMS only, presented in Section IV-C2, where the co-state is fixed to an appropriate constant, the ECMS-based mode determination module of our hierarchical supervisory control algorithm is updated based on the PI controller, as represented in equation (24). In Figure 24, the reason why the change of operating modes appears to be frequent is caused by the power demand and co-state values. Figure 26 represents the results of engine and motor powers determined by the proposed method as well as forecasted power demand using the time-series method in real driving data. The frequency of transition of engine state and transient phenomenon that occurs when switching from the $\chi = 0$ to $\chi = 1$ is reduced.

Based on real driving data with CD-CS mode, the results of NO_x and HC emissions according to the control strategies

TABLE 8. Comparison of NO_x and HC emissions for different control strategies based on real driving data with CD-CS mode.

Control method	Total NO_x [g]	Average NO_x [g/km]
Real driving	73.7533	1.7000
DP	57.0076	1.3139
ECMS only	29.7362	0.6853
Proposed method	51.8255	1.1944

Control method	Total HC [g]	Average HC [g/km]
Real driving	24.5439	0.5657
DP	23.7402	0.5472
ECMS only	22.1932	0.5115
Proposed method	24.8130	0.5719

are shown in Figure 27 and 28, respectively. Table 8 compares NO_x and HC emissions for different supervisory control strategies. The ECMS-only method shows the lowest NO_x and HC emissions. This is because the ECMS-only results in charge-depletion beyond the minimum operation limit, which could degrade the battery performance and life. Compared to the DP solution, the proposed control strategy shows 9.09 % improvement in NO_x emission and 4.52 % degradation in HC emission. Moreover, compared to the real data, the propose method results in 29.73 % improvement in NO_x emission and 1.10 % degradation in HC emission.

4) CONVENTIONAL DRIVING CYCLES

In the previous case studies, the driving cycle used for comparisons of the proposed energy management strategy with the existing methods is of real driving data obtained from real-world commuting drive with a commercial PHEV, in which both urban and highway driving exist and powertrain data is available as well as vehicle speed data. To further demonstrate the effectiveness in saving fuel consumption and reducing greenhouse gas emissions, the proposed hierarchical energy management strategy is applied to two well-known
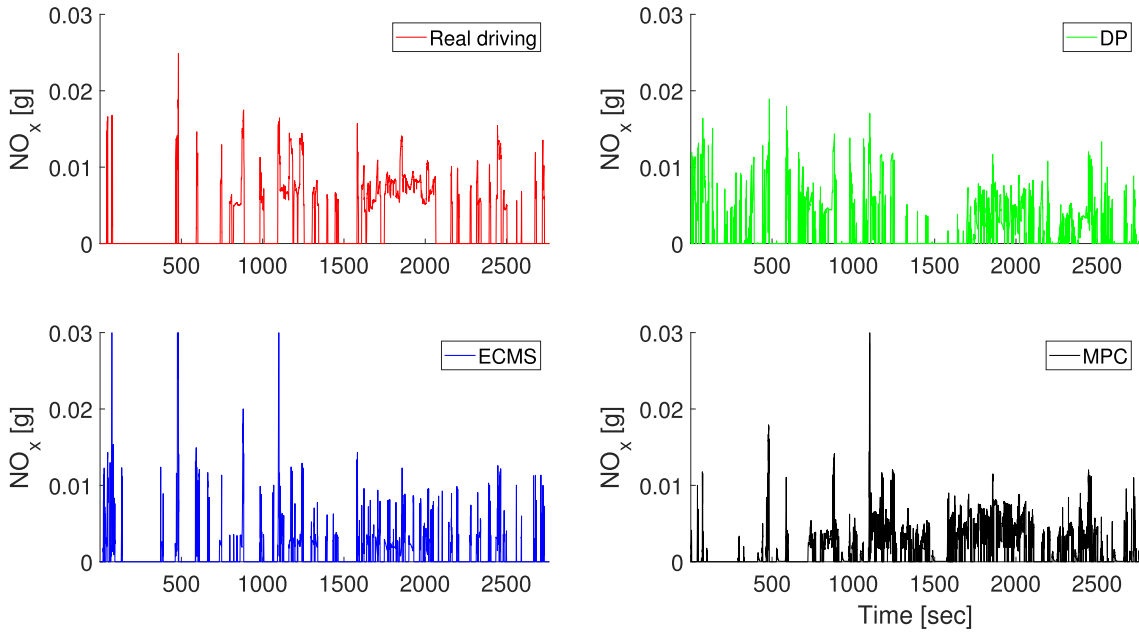
FIGURE 27. A comparison of NO$_x$ emissions determined by control strategies based on real driving data with CD-CS mode.
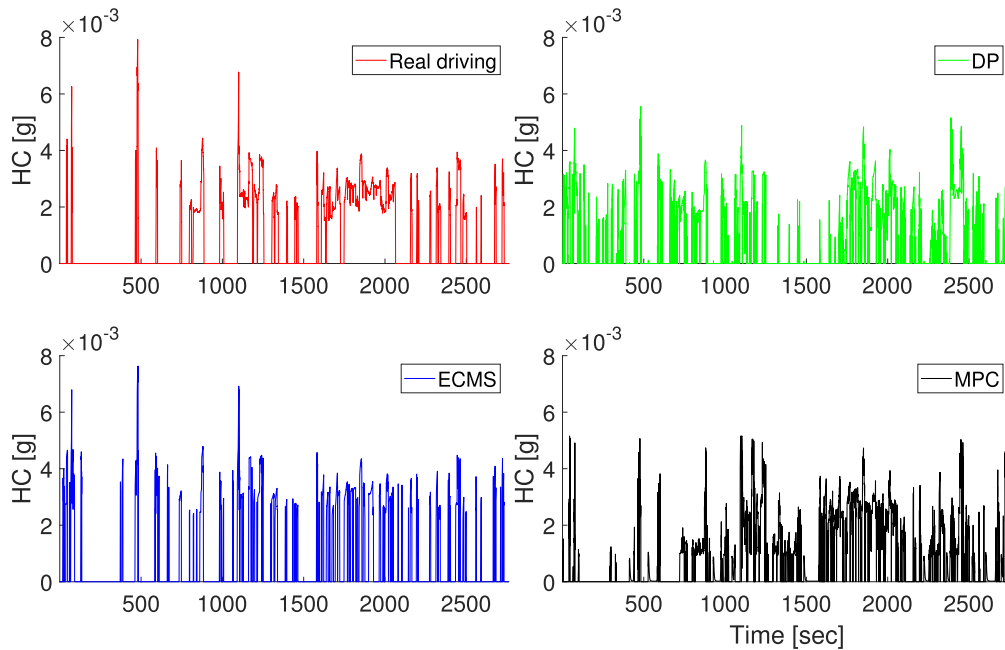

FIGURE 28. A comparison of HC emissions determined by control strategies based on real driving data with CD-CS mode.

conventional driving cycles, HWFET (highway fuel economy test cycle) or FTP-75 (federal test procedure). The speed profiles of these driving cycles are shown in Figure 29.

Since these driving cycles do not have the powertrain data, the demanded traction power for tracking a given speed profile is calculated from the longitudinal dynamics (1) and the formula (3). The computed power-demand profiles are used for training the power-demand prediction module and forecasting the vehicle speed and power-demand. Figures 30 and 31 show the comparisons of the true and predicted vehicle

speed and power-demand for the HWFET and FTP-75 driving cycles, respectively. The normalized RMSE of the predicted vehicle speed and power in test data based on the HWFET and FTP-75 driving cycles are given as follows:

	$\hat{v}_d$	$\hat{P}_d$
HWFET	0.22 %	3.76 %
FTP-75	1.24 %	0.78 %

This error analysis verifies that the proposed method of power-demand prediction can provide fairly accurate
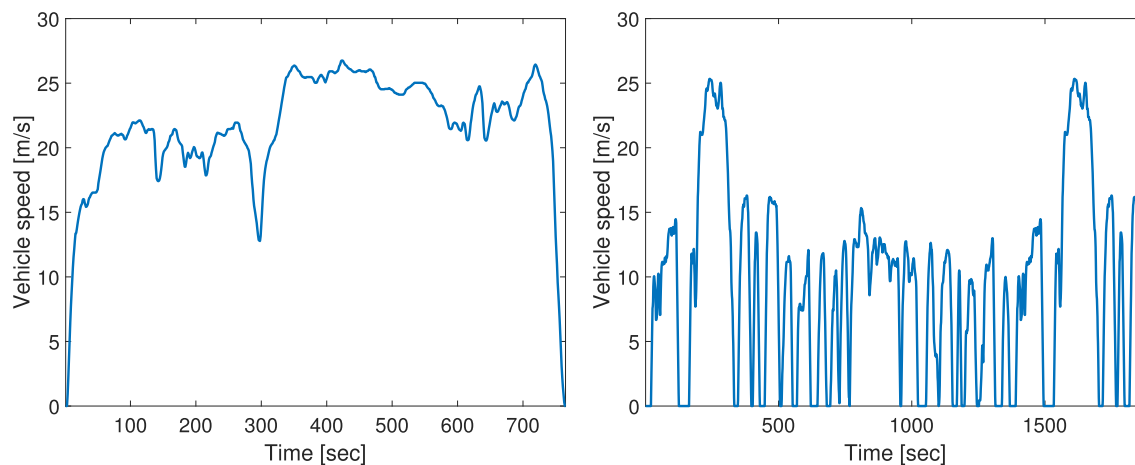
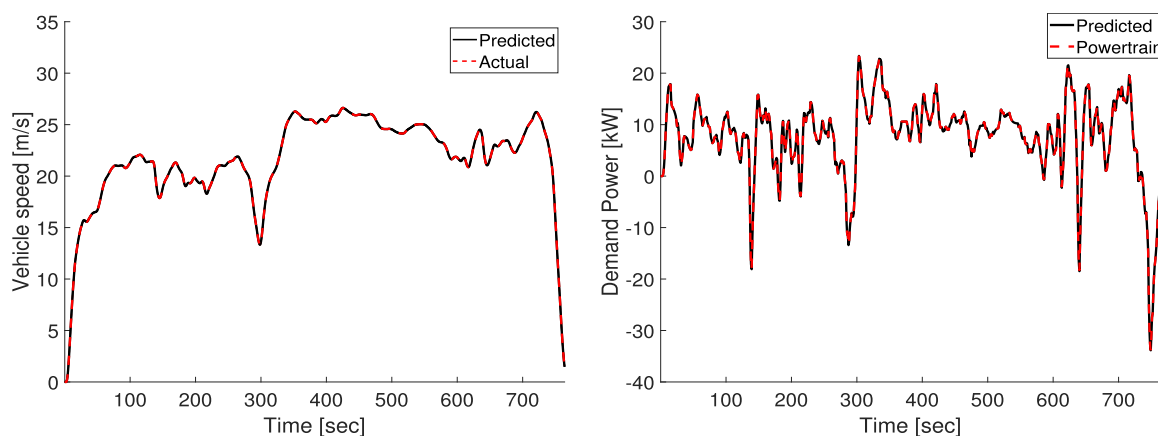**FIGURE 29.** Desired speed for HWFET (left) and FTP-75 (right).

FIGURE 30. Actual vehicle speed/demand-power and forecasted vehicle speed/demand-power by applying time-series method about HWFET driving cycle.
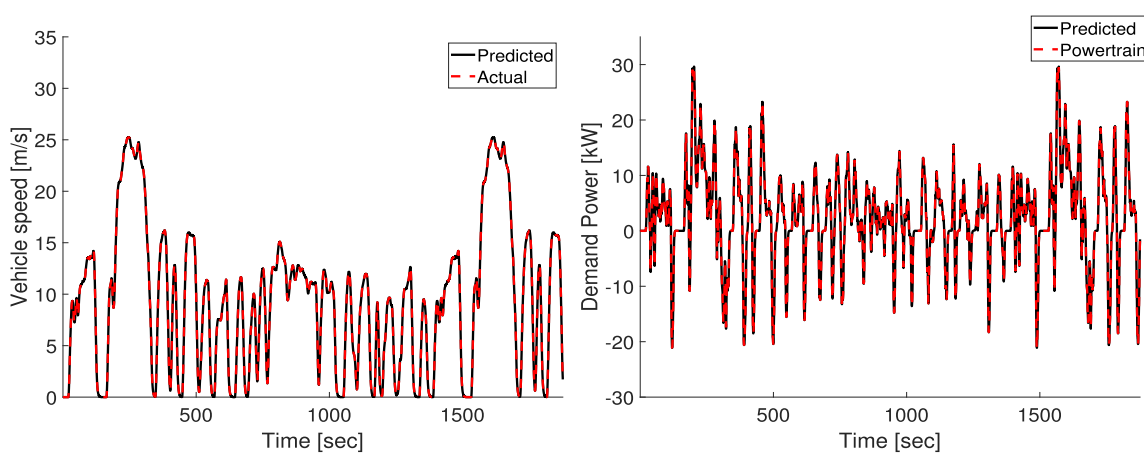
FIGURE 31. Actual vehicle speed/demand-power and forecasted vehicle speed/demand-power by applying time-series method about FTP-75 driving cycle.

forecasting traction-power requests and be used for scheduling dual-source powertrain operation of hybrid electric vehicles.

The proposed optimal energy management strategy is highly dependent on the initial SOC value. We want to investigate the performance of the proposed hierarchical supervisory
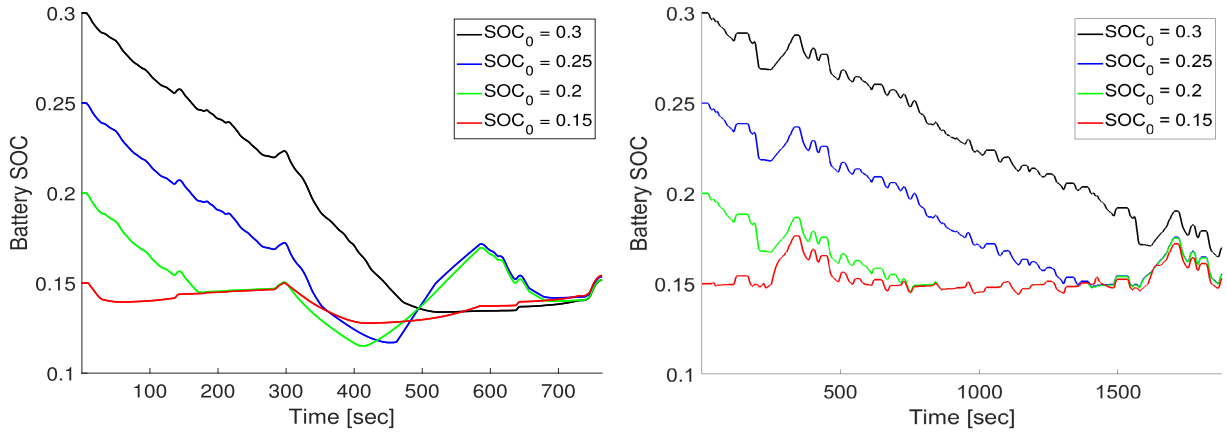
FIGURE 32. Battery SOC according to change of initial value of SOC about HWFET and FTP-75 driving cycle.

TABLE 9. Comparison of NO_x and HC emissions for different ξ_0 based on HWFET driving cycle.

Initial SOC	Total NO_x [g]	Average NO_x [g/km]
$\xi_0 = 0.30$	6.4513	0.3922
$\xi_0 = 0.25$	10.0190	0.6091
$\xi_0 = 0.20$	16.5700	1.0073
$\xi_0 = 0.15$	16.7297	1.0170

Initial SOC	Total HC [g]	Average HC [g/km]
$\xi_0 = 0.30$	3.0234	0.1838
$\xi_0 = 0.25$	5.2024	0.3163
$\xi_0 = 0.20$	6.5455	0.3979
$\xi_0 = 0.15$	7.7812	0.4785

TABLE 10. Comparison of NO_x and HC emissions for different ξ_0 based on FTP-75 driving cycle.

Initial SOC	Total NO_x [g]	Average NO_x [g/km]
$\xi_0 = 0.30$	6.9441	0.3908
$\xi_0 = 0.25$	9.0586	0.5098
$\xi_0 = 0.20$	11.8860	0.6689
$\xi_0 = 0.15$	15.0988	0.8497

Initial SOC	Total HC [g]	Average HC [g/km]
$\xi_0 = 0.30$	2.8609	0.1610
$\xi_0 = 0.25$	4.1760	0.2350
$\xi_0 = 0.20$	6.0280	0.3392
$\xi_0 = 0.15$	7.7312	0.4351

control strategy with varying initial SOC values when driving for the cycles, HWFET and FTP-75, whose total driving distances are 16.45 km and 17.77 km, respectively. Since the driving distances are relatively short, if the initial SOC is about 0.3 then it would operate only with an electric machine. If the initial SOC is lower than 0.3, regenerative braking of the motor is essential to prevent the battery from being discharged when operating only with the motor and the optimal power distribution between motor and engine becomes critical in fuel economy and emission reduction. Figure 32 show the battery SOC profiles with the four different initial SOC values (0.3, 0.25, 0.2, 0.15) resultant from our hierarchical supervisory control algorithm. FTP-75 has a negative sign of demand power periodically, so the motor frequently operates with regenerative braking so that the battery is frequently charged.

In addition to fuel economy, Tables 9 and 10 compare NO_x and HC emissions for different ξ_0 based on HWFET and FTP-75 driving cycles, respectively. For the initial SOC $\xi_0 = 0.3$, the total generated and average values of emission are quite small because it is mainly operated in the charge-depletion mode. On the other hand, for the initial SOC $\xi_0 = 0.2$ or $\xi_0 = 0.15$, the total generated and average values of emission are relatively large because it is mainly operated in the charge-sustaining mode. In conclusion, the simulation results verify that the proposed power management strategy is well applied to conventional driving cycles.

V. CONCLUSION AND FUTURE WORK

In this article, we present a novel method of model-based optimal control for energy management in parallel HEVs. The battery model of an equivalent circuit was utilized to derive a highly nonlinear SOC dynamics model. In addition, the proposed optimal controller explicitly considers the operating limits of battery power and current as well as constraints for the stable and durable operation of the battery. The resultant optimal control problem involved both continuous and discrete control variables corresponding to the motor power and engine clutch, respectively. To avoid expensive computations that might not be feasible in real-time control, we proposed a modularized hierarchical supervisor control architecture that consists of three separate modules: time-series based demand prediction, ECMS-based mode determination, and NMPC-based real-time optimization. Numerical case studies with comparisons to existing supervisory control strategies of HEV for a set of real driving data and several conventional driving cycles illustrate and verify the effectiveness in energy-saving and emission reduction of the proposed real-time optimization-based strategy.

REFERENCES

[1] C. C. Chan, "The state of the art of electric, hybrid, and fuel cell vehicles," *Proc. IEEE*, vol. 95, no. 4, pp. 704–718, Apr. 2007.

[2] K. Ç. Bayindir, M. A. Gözüküçük, and A. Teke, "A comprehensive overview of hybrid electric vehicle: Powertrain configurations, powertrain control techniques and electronic control units," *Energy Convers. Manage.*, vol. 52, no. 2, pp. 1305–1313, 2011.

[3] L. Guzzella and A. Sciarretta, *Vehicle Propulsion Systems: Introduction to Modeling and Optimization*. Berlin, Germany: Springer, 2007.

[4] M. Schori, T. J. Boehme, B. Frank, and M. Schultalbers, "Solution of a hybrid optimal control problem for a parallel hybrid vehicle," *IFAC Proc. Volumes*, vol. 46, no. 21, pp. 109–114, 2013.

[5] M. F. M. Sabri, K. A. Danapalasingam, and M. F. Rahmat, "A review on hybrid electric vehicles architecture and energy management strategies," *Renew. Sustain. Energy Rev.*, vol. 53, pp. 1433–1442, Jan. 2016.

[6] L. Serrao, S. Onori, and G. Rizzoni, "A comparative analysis of energy management strategies for hybrid electric vehicles," *J. Dyn. Syst., Meas., Control*, vol. 133, no. 3, pp. 1–9, May 2011.

[7] Y. Hu, W. Li, K. Xu, T. Zahid, F. Qin, and C. Li, "Energy management strategy for a hybrid electric vehicle based on deep reinforcement learning," *Appl. Sci.*, vol. 8, no. 2, p. 187, Jan. 2018.

[8] S. G. Wirasingha and A. Emadi, "Classification and review of control strategies for plug-in hybrid electric vehicles," *IEEE Trans. Veh. Technol.*, vol. 60, no. 1, pp. 111–122, Jan. 2011.

[9] H.-D. Lee and S.-K. Sul, "Fuzzy-logic-based torque control strategy for parallel-type hybrid electric vehicle," *IEEE Trans. Ind. Electron.*, vol. 45, no. 4, pp. 625–632, Aug. 1998.

[10] H. Hemi, J. Ghouili, and A. Cheriti, "A real time fuzzy logic power management strategy for a fuel cell vehicle," *Energy Convers. Manage.*, vol. 80, pp. 63–70, Apr. 2014.

[11] F. U. Syed, M. L. Kuang, M. Smith, S. Okubo, and H. Ying, "Fuzzy gain-scheduling proportional–integral control for improving engine power and speed behavior in a hybrid electric vehicle," *IEEE Trans. Veh. Technol.*, vol. 58, no. 1, pp. 69–84, Jan. 2009.

[12] P. Zhang, F. Yan, and C. Du, "A comprehensive analysis of energy management strategies for hybrid electric vehicles based on bibliometrics," *Renew. Sustain. Energy Rev.*, vol. 48, pp. 88–104, Aug. 2015.

[13] S. Onori, L. Serrao, and G. Rizzoni, *Hybrid Electric Vehicles: Energy Management Strategies* (Springer Briefs in Electrical and Computer Engineering). London, U.K.: Springer, 2015.

[14] R. Bellman, *Dynamic Programming* (Dover Books on Computer Science). New York, NY, USA: Dover, 2013.

[15] D. Bertsekas, *Dynamic Programming and Optimal Control*. Belmont, MA, USA: Athena Scientific, 2017.

[16] Z. Yuan, L. Teng, S. Fengchun, and H. Peng, "Comparative study of dynamic programming and Pontryagin's minimum principle on energy management for a parallel hybrid electric vehicle," *Energies*, vol. 6, no. 4, pp. 2305–2318, Apr. 2013.

[17] C.-C. Lin, H. Peng, J. W. Grizzle, and J.-M. Kang, "Power management strategy for a parallel hybrid electric truck," *IEEE Trans. Control Syst. Technol.*, vol. 11, no. 6, pp. 839–849, Nov. 2003.

[18] O. Sundström, L. Guzzella, and P. Soltic, "Optimal hybridization in two parallel hybrid electric vehicles using dynamic programming," *IFAC Proc. Volumes*, vol. 41, no. 2, pp. 4642–4647, 2008.

[19] L. Serrao, S. Onori, and G. Rizzoni, "ECMS as a realization of Pontryagin's minimum principle for HEV control," in *Proc. Amer. Control Conf.*, 2009, pp. 3964–3969.

[20] G. Paganelli, S. Delprat, T. M. Guerra, J. Rimaux, and J. J. Santin, "Equivalent consumption minimization strategy for parallel hybrid powertrains," in *Proc. Veh. Technol. Conf., IEEE 55th Veh. Technol. Conf. (VTC Spring)*, vol. 4, May 2002, pp. 2076–2081.

[21] S. Onori, L. Serrao, and G. Rizzoni, "Adaptive equivalent consumption minimization strategy for hybrid electric vehicles," in *Proc. Dyn. Syst. Control Conf.*, vol. 1, 2010, pp. 1–7.

[22] M. Sánchez, S. Delprat, and T. Hofman, "Energy management of hybrid vehicles with state constraints: A penalty and implicit Hamiltonian minimization approach," *Appl. Energy*, vol. 260, Feb. 2020, Art. no. 114149.

[23] C. Yang, S. Du, L. Li, S. You, Y. Yang, and Y. Zhao, "Adaptive real-time optimal energy management strategy based on equivalent factors optimization for plug-in hybrid electric vehicle," *Appl. Energy*, vol. 203, pp. 883–896, Oct. 2017.

[24] C. Sun, F. Sun, and H. He, "Investigating adaptive-ECMS with velocity forecast ability for hybrid electric vehicles," *Appl. Energy*, vol. 185, pp. 1644–1653, Jan. 2017.

[25] J. M. Maciejowski, *Predictive Control: With Constraints*. Upper Saddle River, NJ, USA: Prentice-Hall, 2002.

[26] Y. Huang, H. Wang, A. Khajepour, H. He, and J. Ji, "Model predictive control power management strategies for HEVs: A review," *J. Power Sources*, vol. 341, pp. 91–106, Feb. 2017.

[27] H. Borhan, A. Vahidi, A. M. Phillips, M. L. Kuang, I. V. Kolmanovsky, and S. Di Cairano, "MPC-based energy management of a power-split hybrid electric vehicle," *IEEE Trans. Control Syst. Technol.*, vol. 20, no. 3, pp. 593–603, May 2012.

[28] H. Wang, Y. Huang, A. Khajepour, and Q. Song, "Model predictive control-based energy management strategy for a series hybrid electric tracked vehicle," *Appl. Energy*, vol. 182, pp. 105–114, Nov. 2016.

[29] S. Zhang, R. Xiong, and F. Sun, "Model predictive control for power management in a plug-in hybrid electric vehicle with a hybrid energy storage system," *Appl. Energy*, vol. 185, pp. 1654–1662, Jan. 2017.

[30] X. Lin, Y. Wang, P. Bogdan, N. Chang, and M. Pedram, "Reinforcement learning based power management for hybrid electric vehicles," in *Proc. IEEE/ACM Int. Conf. Comput.-Aided Design (ICCAD)*, Nov. 2014, pp. 33–38.

[31] Y. Zou, T. Liu, D. Liu, and F. Sun, "Reinforcement learning-based real-time energy management for a hybrid tracked vehicle," *Appl. Energy*, vol. 171, pp. 372–382, Jun. 2016.

[32] B. Xu, D. Rathod, D. Zhang, A. Yebi, X. Zhang, X. Li, and Z. Filipi, "Parametric study on reinforcement learning optimized energy management strategy for a hybrid electric vehicle," *Appl. Energy*, vol. 259, Feb. 2020, Art. no. 114200.

[33] R. S. Sutton and A. G. Barto, *Introduction to Reinforcement Learning*, 1st ed. Cambridge, MA, USA: MIT Press, 1998.

[34] J. Wu, H. He, J. Peng, Y. Li, and Z. Li, "Continuous reinforcement learning of energy management with deep q network for a power split hybrid electric bus," *Appl. Energy*, vol. 222, pp. 799–811, Jul. 2018.

[35] X. Han, H. He, J. Wu, J. Peng, and Y. Li, "Energy management based on reinforcement learning with double deep Q-learning for a hybrid electric tracked vehicle," *Appl. Energy*, vol. 254, Nov. 2019, Art. no. 113708.

[36] T. Nüesch, A. Cerofolini, G. Mancini, N. Cavina, C. Onder, and L. Guzzella, "Equivalent consumption minimization strategy for the control of real driving NOx emissions of a diesel hybrid electric vehicle," *Energies*, vol. 7, no. 5, pp. 3148–3178, 2014.

[37] V. Madanipour, M. Montazeri-Gh, and M. Mahmoodi-K, "Multi-objective component sizing of plug-in hybrid electric vehicle for optimal energy management," *Clean Technol. Environ. Policy*, vol. 18, no. 4, pp. 1189–1202, 2016.

[38] M. Montazeri-Gh and M. Mahmoodi-K, "Optimized predictive energy management of plug-in hybrid electric vehicle based on traffic condition," *J. Cleaner Prod.*, vol. 139, pp. 935–948, Dec. 2016.

[39] C. Zhang, D. Wang, B. Wang, and F. Tong, "Battery degradation minimization-oriented hybrid energy storage system for electric vehicles," *Energies*, vol. 13, no. 1, pp. 246–276, 2020.

[40] Y. Wang, X. Jiao, Z. Sun, and P. Li, "Energy management strategy in consideration of battery health for PHEV via stochastic control and particle swarm optimization algorithm," *Energies*, vol. 10, no. 11, pp. 1894–1914, 2017.

[41] A. Cordoba-Arenas, S. Onori, and G. Rizzoni, "A control-oriented lithium-ion battery pack model for plug-in hybrid electric vehicle cycle-life studies and system design with consideration of health management," *J. Power Sources*, vol. 279, pp. 791–808, Apr. 2015.

[42] R. Rajamani, *Vehicle Dynamics and Control*, 2nd ed. New York, NY, USA: Springer, 2011.

[43] D. Ambuhl and L. Guzzella, "Predictive reference signal generator for hybrid electric vehicles," *IEEE Trans. Veh. Technol.*, vol. 58, no. 9, pp. 4730–4740, Nov. 2009.

[44] M. Cipek, D. Pavković, and J. Petrić, "A control-oriented simulation model of a power-split hybrid electric vehicle," *Appl. Energy*, vol. 101, pp. 121–133, Jan. 2013.

[45] O. Sundstrom, "Optimal control and design of hybrid electric vehicles," Ph.D. dissertation, ETH Zürich, Zürich, Switzerland, 2009.

[46] W. Li, G. Xu, Z. Wang, and Y. Xu, "Dynamic energy management for hybrid electric vehicle based on approximate dynamic programming," in *Proc. 7th World Congr. Intell. Control Automat.*, 2008, pp. 7864–7869.

[47] A. Vogel, D. Ramachandran, R. Gupta, and A. Raux, "Improving hybrid vehicle fuel efficiency using inverse reinforcement learning," in *Proc. 26th AAAI Conf. Artif. Intell.*, 2012, pp. 384–390.

[48] C. Sun, S. J. Moura, X. Hu, J. K. Hedrick, and F. Sun, "Dynamic traffic feedback data enabled energy management in plug-in hybrid electric vehicles," *IEEE Trans. Control Syst. Technol.*, vol. 23, no. 3, pp. 1075–1086, May 2015.

[49] Q. Gong, Y. Li, and Z.-R. Peng, "Trip-based optimal power management of plug-in hybrid electric vehicles," *IEEE Trans. Veh. Technol.*, vol. 57, no. 6, pp. 3393–3401, Nov. 2008.
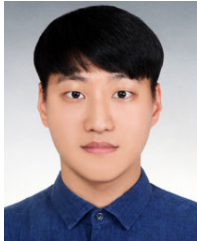
JINSUNG KIM received the B.S. and M.S. degrees in electrical and computer engineering from Inha University, Incheon, South Korea, in 2018 and 2020, respectively. He is currently a Research Engineer with the Laboratory for Control and Information Systems, Inha University. His research interests include optimal control and model predictive control with application to power electronics, power systems, and electrified vehicles.

HOONHEE KIM received the B.S. degree in electrical engineering from Inha University, Incheon, South Korea, in 2019, where he is currently pursuing the M.S. degree in electrical and computer engineering. His research interests include optimal control and model predictive control with application to electrified vehicle control.

JINWOO BAE received the B.S. degree in electronic physics from Kwangwoon University, Seoul, South Korea, in 2017. He is currently pursuing the M.S. degree in electrical and computer engineering with Inha University, Incheon, South Korea. From 2017 to 2018, he has worked as a Field Service Engineer with Canon Semiconductor Engineering Korea. His research interests include optimal control and dynamic programming and reinforcement learning with application to automotive and robotics.

DOHEE KIM received the B.S. degree in natural sciences and the M.S. degree in astronomy and space science from Yonsei University, in 2006 and 2008, respectively, and the Ph.D. degree in mechanical and aerospace engineering from the University of Florida, in 2011. He has been a Senior Research Engineer with the Electrified Systems Control Research Laboratory, Hyundai Motor Company, since 2012. His research interests include nonlinear control, adaptive control, optimal control, and model predictive control with practical applications to electrified vehicles, spacecrafts, and robotics.

JEONG SOO EO (Member, IEEE) received the B.S. degree in electronics engineering from Korea University, in 1994, and the M.S. degree in electrical and computer engineering from The University of Texas at Austin, in 2005. He joined Hyundai Motor Company, in 1993, where he has been a Research Fellow with the Electrified Systems Control Research Laboratory, since 2019. His research interests include observer-based control, nonlinear control, and optimal control for (P)HEV and EV, software testing method, and on-board diagnosis systems for internal combustion engine.

KWANG-KI K. KIM received the M.S. and Ph.D. degrees in aerospace engineering from the University of Illinois at Urbana–Champaign, Champaign, IL USA, in 2009 and 2013, respectively. From 2013 to 2016, he was a Postdoctoral Fellow affiliated with the School of Electrical and Computer Engineering, Georgia Institute of Technology. He has worked as a Senior Research Engineer with the Electronics Technology Center, Hyundai Motor Company. He joined Inha University, in 2017, where he has been an Assistant Professor with the Department of Electrical Engineering, since 2017. His research interests include learning and optimization for control, nonlinear control, robust control, networked control, optimal control, game-theoretic approaches to distributed control with practical applications to real-time planning and control of electrified vehicles, reinforcement learning for robotics, model predictive control for power electronics control, and power system optimization.

● ● ●